# Stony Brook University

# The Influence of Disorder on Bloch Oscillations in a System of Ultracold Atoms in an Optical Lattice

A Thesis Presented

by

**Stefan Walter**

to

The Graduate School

in Partial Fulfillment of the Requirements

for the Degree of

**Master of Arts**

in

**Physics**

Stony Brook University

August 2009

**Stony Brook University**

The Graduate School

## Stefan Walter

We, the thesis committee for the above candidate for the Master of Arts degree, hereby recommend acceptance of this thesis.

Adam C. Durst – Thesis Advisor
Assistant Professor, Department of Physics and Astronomy

Thomas Tzu Szu Kuo – Chairperson of Defense
Professor, Department of Physics and Astronomy

Dominik Schneble
Assistant Professor, Department of Physics and Astronomy

This thesis is accepted by the Graduate School.

Lawrence Martin
Dean of the Graduate School

Abstract of the Thesis

# The Influence of Disorder on Bloch Oscillations in a System of Ultracold Atoms in an Optical Lattice

by

**Stefan Walter**

**Master of Arts**

in

**Physics**

Stony Brook University

2009

During the last decade ultracold atoms in optical lattices have become a great experimental tool for studying quantum systems. The topic that is being addressed in this thesis, is inspired from a solid state point of view. Crystals are a periodic system and it is easy to describe the transport of electrons in such a periodic system.However, the perfect periodic crystal is rarely realized in nature. Impurities and defects, which lead to a disorder of the periodic system are always present. This disorder affects for instance the transport of electrons in the crystal. A system of ultracold atoms in an optical lattice gives an instrument to resemble the perfectly periodic crystal. In recent years the possibility to realize disorder experimentally in an optical lattice has emerged. This allows one to address many new questions on the influence of disorder in such systems. In this thesis we are especially interested in the dynamics of a wave packet in such a disordered system.

The dynamics which are investigated in this work are Bloch os-

cillations in a disordered system of ultracold atoms in an optical lattice. We use numerical simulations to solve the time dependent Schrödinger equation. After having solved the Schrödinger equation for the wave function, the dynamics of the system, perfectly periodic or disordered, can be explored.

As a result of disorder in the system, the Bloch oscillations get damped, and a dependance of the damping on the parameters qualifying the disorder is being established.

An interesting effect in a disordered optical lattice with interaction between atoms in neighboring wells, is that increasing the interaction, leads to a decrease in the damping of the Bloch oscillations caused by disorder. This effect is covered in the last part of the thesis.

To Maria.

# Contents

**List of Figures** . . . viii

**List of Tables** . . . x

**Acknowledgements** . . . xi

**1 Introduction** . . . 1

**2 Properties of particles in a crystal** . . . 3
2.1 Bloch's Theorem . . . 3
2.2 The cosine-potential . . . 5
2.3 Dynamics of particles in a periodic potential . . . 6
2.4 Wannier-Stark ladders . . . 10

**3 Bose-Einstein Condensates** . . . 11
3.1 The Gross-Pitaevskii equation . . . 11
3.2 The one dimensional Gross-Pitaevskii equation . . . 13
3.3 The optical lattice . . . 14
3.4 Realization of disorder in an optical lattice . . . 17
3.4.1 Disorder introduced by an incommensurate potential . . . 18
3.4.2 Disorder introduced by an atomic mixture . . . 19

**4 Numerical results** . . . 21
4.1 Bloch oscillations in optical lattices . . . 21
4.2 Disorder in optical lattices introduced by an additional potential 23
4.2.1 Changing the ratio $\alpha$ between the two optical lattices . . . 24
4.2.2 Changing the depth $V_0$ of the optical lattices . . . 30
4.2.3 Changing the amplitude $s$ of the disorder potential . . . 31
4.2.4 Analytical Approach . . . 32
4.3 Disorder introduced by impurities at distinct lattice sites . . . 35
4.3.1 Patterns of impurities . . . 36

4.3.2 Randomly distributed impurities . . . . . 38
4.4 Mechanism of the damping . . . . . 42
4.5 Disorder and interaction . . . . . 43

**5 Conclusion** . . . . . 50

**Bibliography** . . . . . 51

**A Units** . . . . . 55
A.1 Units used for numerical calculations . . . . . 55

**B Numerical methods** . . . . . 57
B.1 Solving the stationary Schrödinger equation for Bloch bands and Bloch functions . . . . . 57
B.2 The Split Operator Method . . . . . 61
B.3 The Split Operator Technique for the nonlinear Schrödinger equation . . . . . 63

# List of Figures


2.1 Band structure for a cosine-potential . . . . . 6
2.2 Motion of an electron in $k$-space under the influence of an external field $F$ . . . . . 8
2.3 Tilted bands . . . . . 9

3.1 Band structure for a $10\,E_R$ deep optical lattice . . . . . 17
3.2 Two kinds of realizations of disorder in an optical lattice . . . 20

4.1 Density $|\psi_0(x,t)|^2$ and $|\psi_p(x,t)|^2$ as a function of position and time . . . . . 22
4.2 Undamped Bloch oscillations . . . . . 24
4.3 Damped Bloch oscillations . . . . . 25
4.4 Mean width $\Delta\sigma$ of a wave packetin a disordered system . . . . 25
4.5 Damping of Bloch oscillations as a function of $\alpha$ and $s = 0.0005$ 27
4.6 $\langle x(t)\rangle$ and band structure for $\alpha = 0.5$ and $s = 0.0005$ . . . . . 28
4.7 Motion in a system with two periodic potential with $s = 0.0005$ and $\alpha = 0.5$ . . . . . 28
4.8 Overlap $|\,\langle\psi(x,t=0)|\psi(x,t)\rangle\,|$ for $\alpha = 0.5$ . . . . . 29
4.9 The regions around $\alpha = 0.5$ and $\alpha = 1.5$ enlarged . . . . . 30
4.10 Damping of Bloch oscillations for different depths of the optical lattice at $s = 0.0005$ . . . . . 31
4.11 Damping of Bloch oscillations for different disorder strengths $s$ 32
4.12 Exact numerical results compared to a tight binding model . . 35
4.13 Bloch oscillations in a system with an impurity on every other lattice site . . . . . 37
4.14 Bloch oscillations in a system with a slightly periodic pattern of impurities . . . . . 37
4.15 $\langle x(t)\rangle$ for randomly distributed impurities . . . . . 40
4.16 Overlap of the wave function for the case of randomly distributed impurities . . . . . 41
4.17 Density $|\psi(k,t)|^2$ with and without disorder . . . . . 42
4.18 Damped Bloch oscillations in a system with interactions . . . 44

4.19 Interplay between disorder and interaction . . . . . 45

# List of Tables

4.1 Summary on amplitudes $A_{BO}$ for different lattice depths $V_0$ . . 30

A.1 Summary of used parameters . . . . . 56

B.1 Summary of arguments . . . . . 58

# Acknowledgements

The past year at Stony Brook, would have not been possible without the great exchange program from the University of Würzburg and its organization by Fakher Assaad. I am very grateful for the financial support from the DAAD which made things a lot easier.

During the last I had great support from all different kinds of people, here at Stony Brook, as well as at home in Germany.

First there is Adam Durst, my advisor, who I would like to thank for giving me the opportunity to work in his group. I enjoyed working on the interesting topic he has given me. Adam was always very supportive, not only on our weekly meetings, but also when I just came by his office he gave me new input.

I also would like to thank Dominik Schneble for taking time to look at my work and providing new ideas to it.

I am very glad to have a family like mine at home who is supporting me no matter what the circumstances. Knowing I can count on them, no matter what I am going to do is very comforting.

At last I want to thank the most important person, Maria. I am incredible lucky to have someone like you. I can't take what you did for me for granted, and I do not know how to thank you for that. I can't wait to see you again.

# Chapter 1

# Introduction

The dynamics of electrons in the periodic potential of a crystalline solid exposed to an external homogeneous field has been an important problem in solid state physics since the paper of Bloch in 1928 [1]. In contrast to an expected uniform acceleration these electrons oscillate in coordinate as well as in momentum space. These oscillations are called Bloch oscillations. However, Bloch oscillations are not observable in crystals because the characteristic scattering time $\tau$ for electrons due to impurities is shorter than the period of the Bloch oscillations. In the 1970s, the fabrication of semiconductor superlattices which are a controllable one-dimensional periodic system lead to the direct observation of Bloch oscillations [2–4]. In recent years ultracold atoms in optical lattices have provided an exceptional experimental tool for studying phenomena which have their origin in solid state physics. Optical lattices are an analogue to the perfect pure crystal and have been used to study a great variety of solid state problems. Bloch oscillations have been observed in [5–11], Wannier-Stark ladders were studied in [12] and Zener-tunneling was investigated in [13, 14].

The great advantage of optical lattices is the possibility to modify the potential with great freedom. The depth of the potential wells, the interaction between atoms in adjacent wells and the force of the external field can be adjusted easily. This system also inherits the possibility to place "impurities" on certain lattice sites. Systems with two competing periodic potentials generated by two standing laser waves can also be realized. In this case one laser generates the actual optical lattice and the other one plays the role of disorder. These two lasers could be commensurate or incommensurate in their wavelengths.

One goal of this thesis is to investigate the influence of impurities on Bloch oscillations in optical lattices including weather a periodic pattern of impurities shows Bloch oscillations and what happens if impurities are randomly placed

in the optical lattice.

Another goal will be the study of an optical lattice with two competing periodic potentials. These systems represent a very controlled way to introduce disorder in an optical lattice. For this kind of disorder, the dependance of the damping of Bloch oscillations on the parameters which describe the disorder, is being explored.

In an optical lattice, atoms in neighboring wells also interact with each other. This interaction alone will lead to a damping of Bloch oscillations. However, in the case of a disordered system, these interactions can counteract the damping of Bloch oscillations due to the disorder. This interesting interplay between interaction and disorder will also be investigated in this thesis.

The main instrument for studying these effects is the numerical simulation of the time dependent Schrödinger equation with a potential that describes the disorder. The simulation of the Schrödinger equation resembles the actual experimental situation very well.

# Chapter 2

# Properties of particles in a crystal

## 2.1 Bloch's Theorem

The optical lattice is equivalent to a perfectly pure crystal where the potential is given by the atoms in the crystal. It is therefore necessary to review the formalism borrowed from solid state physics to describe the properties of electrons in a periodic potential, as for instance done in [15]. In the following we examine the one-dimensional case of a periodic potential, which can easily be generalized to three dimensions. The Schrödinger equation for an electron in a one-dimensional potential $V(x)$ is given by

$$\left[-\frac{\hbar^2}{2m}\frac{\partial^2}{\partial x^2} + V(x)\right]\psi(x) = E\,\psi(x)\,. \tag{2.1}$$

Solutions of Eq. (2.1) for different kinds of potentials, *e. g.* $V(x) = 0$ (free electron case), $V(x) = Kx^2/2$ (harmonic oscillator), $V(x) = e\epsilon x$ (uniform electric field $\epsilon$), etc. are well known. A special kind of potential, which is of interest in solid state physics, is the periodic potential

$$V(x + ma) = V(x)\,, \tag{2.2}$$

with $a$ being the period of the potential and $m$ being an integer. Electrons in such a periodic potential are called *Bloch electrons*. From the periodicity of the potential it follows that its Fourier expansion only includes plane waves

with wavenumbers $K_n = \frac{2\pi}{a}\, n$, which is a reciprocal lattice vector:

$$V(x) = \sum_{n=-\infty}^{\infty} V_n\, e^{iK_n x}\,. \tag{2.3}$$

In the special case of free electrons, $V(x) = 0$ in Eq. (2.1), the wave functions are plane waves of the form

$$\psi_k(x) = \frac{1}{\sqrt{L}}\, e^{ikx}\,, \tag{2.4}$$

with $\psi_k(x)$ normalized to 1 in the interval $0 \le x \le L$ where $L$ denotes the length of the crystal. The corresponding eigenvalues are

$$E(k) = \frac{\hbar^2 k^2}{2m}\,. \tag{2.5}$$

The plane waves in Eq. (2.4) are an orthonormal set of functions and can therefore be used as an expansion set. Using the Fourier expansion of the periodic potential and the plane waves as a basis, we can write Eq. (2.1) as

$$\left[-\frac{\hbar^2}{2m}\,(k-K)^2 - E\right] c_{k-K} + \sum_{K'} V_{K'-K}\, c_{k-K'} = 0\,. \tag{2.6}$$

Eq. (2.6) is a matrix equation for each allowed $k$-value in the first Brillouin zone. Since $k$ is restricted to the first Brillouin zone, $k \in [-\pi/a,\, \pi/a]$, only coefficients $c_k, c_{k-K_1}, c_{k-K_2}, ...$ (which lie outside the first Brillouin zone) are coupled, leading to an independent set of equations for each $k$ in the first Brillouin zone. The secular equation in Eq. (2.6) can be diagonalized for each $k$, and the obtained eigenvectors lead to the eigenfunctions of the system, which can be written as

$$\phi_{n,k}(x) = \sum_{K} c^n_{k-K}\, e^{i(k-K)x} \tag{2.7}$$

$$= e^{ikx} \sum_{K} c^n_{k-K}\, e^{-iKx}\,, \tag{2.8}$$

where $n$ is the band index. This leads us to the result

$$\phi_{n,k}(x) = e^{ikx}\, u_{n,k}(x)\,, \tag{2.9}$$

with $u_{n,k}(x+a) = u_{n,k}(x)$ having the same periodicity as the potential. Eq. (2.9) is called *Bloch's theorem*. Another way of writing *Bloch's theorem* is

$$\phi_{n,k}(x+ma) = e^{ikma}\,\phi_{n,k}(x)\,, \tag{2.10}$$

where $ma$ is a translation by multiples of the lattice constant. The eigenvalues of the secular equation in Eq. (2.6) are the energy values $E_{n,k}$ for each $k$. Both, the Bloch functions $\phi_{n,k}(x)$ and the energy values $E_{n,k}$ have the periodicity of the reciprocal lattice

$$\phi_{n,k+K}(x) = \phi_{n,k}(x) \tag{2.11}$$

$$E_{n,k+K} = E_{n,k}\,. \tag{2.12}$$

In the next section we will show how the Hamiltonian matrix is computed for the cosine-potential, which is used throughout this work.

## 2.2 The cosine-potential

For what follows, we choose the periodic potential in Eq. (2.1) to be a cosine-potential $V(x) = V_0\cos(\frac{2\pi}{a}x)$. With this choice we can easily compute the matrix elements of the Hamiltonian Eq. (2.1) in a plane wave basis. The starting point is the Hamiltonian

$$H = -\frac{\hbar^2}{2m}\frac{\partial^2}{\partial x^2} + V_0\cos(\frac{2\pi}{a}\,x)\,. \tag{2.13}$$

The expansion of the wave function to this Hamiltonian in plane waves reads

$$\omega_n(x) = \frac{1}{\sqrt{L}}\,e^{i(k-K_n)x}\,. \tag{2.14}$$

We can evaluate the matrix elements of the Hamiltonian Eq. (2.13) in the following way,

$$\langle\omega_m(x)|\,H\,|\omega_n(x)\rangle = \frac{\hbar^2\,(k-K_n)^2}{2m}\,\delta_{m,n} + \frac{1}{L}\int_0^L dx\,e^{-i(K_m-K_n)x}\,V_0\cos(\frac{2\pi}{a}\,x) \tag{2.15}$$

$$= \frac{\hbar^2\,(k-K_n)^2}{2m}\,\delta_{m,n} + \frac{V_0}{2}\,(\delta_{m,n+1}+\delta_{m,n-1})\,. \tag{2.16}$$

The diagonalization of $H$ yields the following secular equation for the energy eigenvalues $E$

$$\left[\frac{\hbar^2 (k - K_n)^2}{2m} - E\right] \delta_{n,m} + \frac{V_0}{2} (\delta_{m,n+1} + \delta_{m,n-1}) = 0 \,. \tag{2.17}$$

Fig. 2.1 shows a plot of $E_n(k)$ as a result of diagonalizing Eq. (2.13). App. A.1 describes how to compute the band structure numerically.

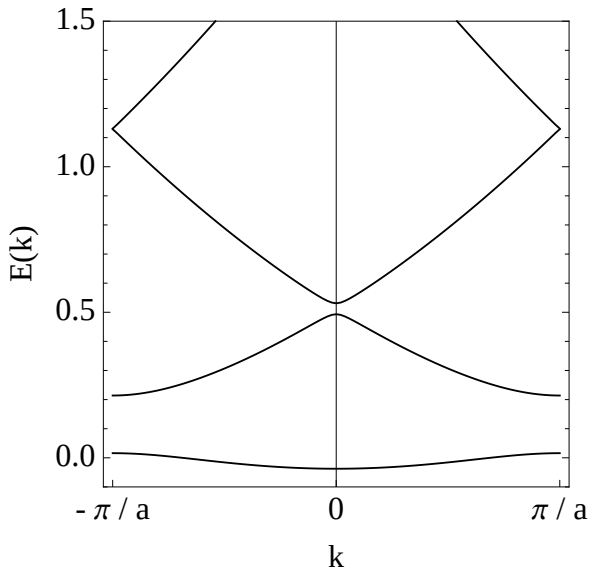


Figure 2.1: **Band structure for a cosine-potential.** To illustrate the band structure of a periodic potential, the energy bands in the first Brillouin zone are shown.

## 2.3 Dynamics of particles in a periodic potential

The first quantity of interest is the electron velocity $v(k)$, which is given by

$$v(k) = \langle \phi_{n,k}(x) | \frac{p}{m} | \phi_{n,k}(x) \rangle \,. \tag{2.18}$$

We start from

$$\langle \phi_{n,k}(x)| \frac{p^2}{2m} + V(x) |\phi_{n,k}(x)\rangle = E_n(k) \tag{2.19}$$

$$\left\langle e^{-ikx} u_{n,k}(x)\right| \frac{p^2}{2m} + V(x) \left|e^{ikx} u_{n,k}(x)\right\rangle = E_n(k) \tag{2.20}$$

$$\langle u_{n,k}(x)| \frac{(p+\hbar k)^2}{2m} + V(x) |u_{n,k}(x)\rangle = E_n(k)\,, \tag{2.21}$$

and take the derivative of Eq. (2.21) with respect to $k$ which yields

$$\langle u_{n,k}(x)| \frac{\hbar(p+\hbar k)}{m} |u_{n,k}(x)\rangle = \frac{dE_n(k)}{dk} \tag{2.22}$$

$$\langle \phi_{n,k}(x)| \frac{\hbar p}{m} |\phi_{n,k}(x)\rangle = \frac{dE_n(k)}{dk}\,. \tag{2.23}$$

Together with Eq. (2.18) we arrive at the well known expression for an electron's velocity:

$$v(k) = \frac{1}{\hbar}\frac{dE_n(k)}{dk}\,. \tag{2.24}$$

Under the influence of an external uniform electric field $\epsilon$ the Hamiltonian in Eq. (2.1) becomes

$$H = -\frac{\hbar^2}{2m}\frac{\partial^2}{\partial x^2} + V(x) + e\epsilon x\,, \tag{2.25}$$

where $e$ is the electronic charge. The time evolution of an initial state prepared as a Bloch state $\phi_{n,k_0}(x,0)$ is then given by

$$\phi(x,t) = e^{-\frac{i}{\hbar}\left(\frac{p^2}{2m}+V(x)+e\epsilon x\right)t} \phi_{n,k_0}(x,0)\,. \tag{2.26}$$

Performing a translation $x \to x+a$ leads us to

$$\phi(x+a,t) = e^{-\frac{i}{\hbar}\left(\frac{p^2}{2m}+V(x+a)+e\epsilon(x+a)\right)t} \phi_{n,k_0}(x+a,0) \tag{2.27}$$

$$= e^{-\frac{i}{\hbar}\left(\frac{p^2}{2m}+V(x)+e\epsilon x\right)t} e^{-\frac{i}{\hbar}e\epsilon a t} e^{ik_0 a} \phi_{n,k_0}(x,0) \tag{2.28}$$

$$= e^{-\frac{i}{\hbar}\left(\frac{p^2}{2m}+V(x)+e\epsilon x\right)t} e^{i(-\frac{e\epsilon t}{\hbar}+k_0)a} \phi_{n,k_0}(x,0) \tag{2.29}$$

$$= e^{ik(t)a}\phi(x,t)\,. \tag{2.30}$$

The result is that the wave function is a Bloch-type wave function with a time

dependent function $k(t)$, which evolves linearly with time according to

$$k(t) = -\frac{1}{\hbar} e\epsilon t + k_0 \,, \tag{2.31}$$

or in the form of the well known acceleration theorem:

$$\frac{d(\hbar k)}{dt} = -e\epsilon \,. \tag{2.32}$$

If we now restrict the electron only to be in the first band, *i. e.* neglecting Zener-tunneling [16], the motion of the electron is governed by Eq. (2.31) and Eq. (2.24). Fig. 2.2 shows the schematic time evolution in the band picture for the free electron case (left) and for a periodic potential (right). In the case

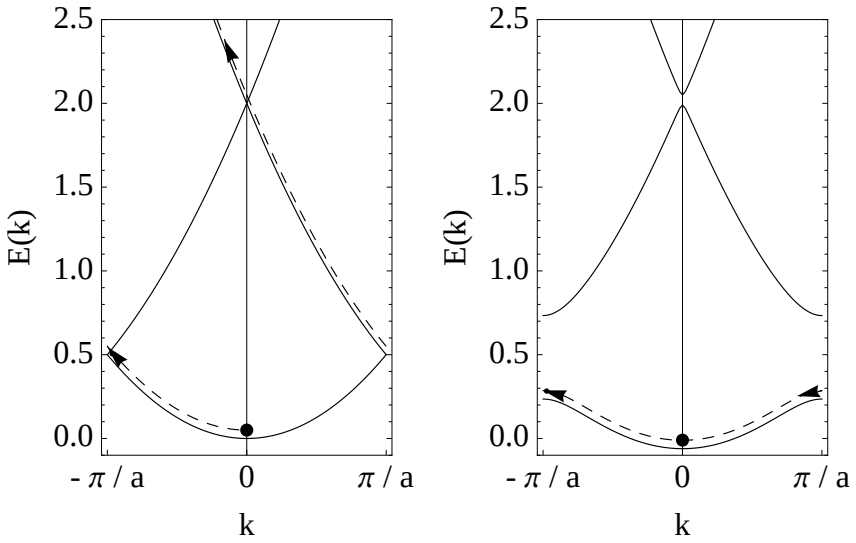


Figure 2.2: **Motion of an electron in *k*-space under the influence of an external field *F*.** Left: In the free electron case ($V(x) = 0$), the electron's momentum, velocity and energy are increasing infinitely with time. Right: In the case of a periodic potential the band structure shows energy gaps between Bloch bands. Neglecting the tunneling to higher bands, the electron performs an oscillating motion in the lowest Bloch band.

of a periodic potential and an additional external field, the electron performs a periodic motion in momentum space as well as in real space. The period

of these oscillations can be obtained from Eq. (2.31) by the assumption that it takes the electron the time $T_B$ to cross the whole Brillouin zone (distance $2\pi/a$)

$$T_B = \frac{2\pi\hbar}{ae\epsilon}\,. \tag{2.33}$$

The amplitude $A'$ of the Bloch oscillations can be obtained by the simple tilted band picture of Zener, see Fig. 2.3. The whole space available for the oscillations $A$, can in this picture be determined as

$$A = \frac{\Delta}{e\epsilon}\,, \tag{2.34}$$

where $\Delta$ is the bandwidth of the band, in which the oscillation is considered. The amplitude is $A' = A/2$ due to symmetry. In this whole derivation the

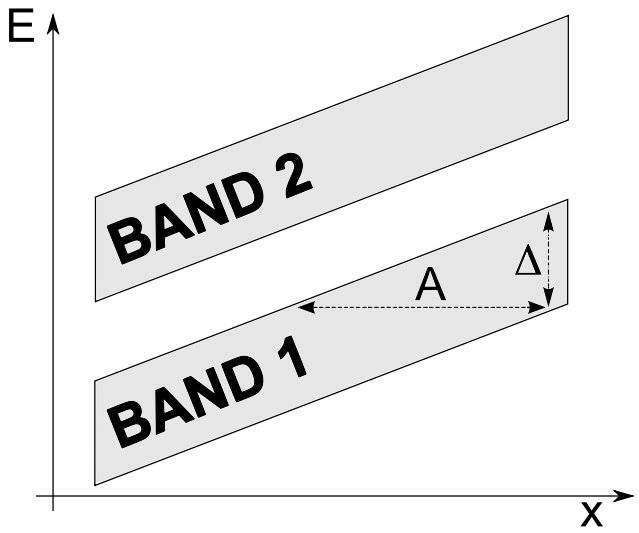


Figure 2.3: **Tilted bands.** The bandwidth $\Delta$ can be calculated and the slope $e\epsilon$ is given by the strength of the electric field $\epsilon$, this leads to the space covered by the Bloch oscillations in real space.

perfectly periodic pure crystal was considered, but in reality, electrons in a crystal are being scattered from impurities. The average time between two collisions is called $\tau$. This means that Bloch oscillations in a real crystal can only be observed if the time $\tau$ between two collisions is larger than the Bloch period $T_B$. This condition is not satisfied in real crystals, which means no Bloch oscillations are observed. The first experimental realization of systems, which show observable Bloch oscillations were semiconductor superlattices.

These systems have a larger lattice constant $a$, which decreases the Bloch period and they also have a larger characteristic scattering lifetime $\tau$. As a consequence, the condition $T_B < \tau$ could be satisfied in these systems.

## 2.4 Wannier-Stark ladders

To give a complete description of phenomena occurring in a periodic lattice, if an external homogeneous field is applied, we give a short description of the Wannier-Stark ladder. The first description of this problem was given by Wannier in 1960 [17], followed by a long controversy on the topic. The history is well summarized in [18, 19].

Due to the external field the translation invariance of the system is broken and the band picture has to be abandoned. However, there can be found another quantization which is called the Wannier-Stark ladder. Given that the stationary Schrödinger equation plus external electric field has eigenfunctions $\Psi(x)$ with corresponding eigenvalues $E$

$$\left[-\frac{\hbar^2}{2m}\frac{\partial^2}{\partial x^2} + V(x) + e\epsilon x\right]\Psi(x) = E\,\Psi(x)\,, \tag{2.35}$$

a translation $x \to x + ma$ in Eq. (2.35) leads us to:

$$\left[-\frac{\hbar^2}{2m}\frac{\partial^2}{\partial x^2} + V(x) + e\epsilon x\right]\Psi(x + ma) = (E + mae\epsilon)\;\Psi(x + ma)\,. \tag{2.36}$$

We rewrite Eq. (2.36) in the following form

$$\left[-\frac{\hbar^2}{2m}\frac{\partial^2}{\partial x^2} + V(x) + e\epsilon x\right]\Psi_{\mu,m}(x) = E_{\mu,m}\,\Psi_{\mu,m}(x)\,, \tag{2.37}$$

with $E_{\mu,m} = E_{\mu,0} + mae\epsilon$ being the Wannier-Stark ladder and $\Psi_{\mu,m}(x) = \Psi_{\mu,0}(x + ma)$ being the Wannier-Stark states. As a result the solutions to Eq. (2.35) are quantized in ladders with rungs separated by $mae\epsilon$, where $m$ is an integer denoting the lattice site and $\mu$ is the ladder index. The description of a tilted lattice in terms of Wannier-Stark states could be used to gain insight into the tunneling probability of a wave function to higher bands, enhanced by a strong external electric field $\epsilon$.

# Chapter 3

# Bose-Einstein Condensates

As previously mentioned, the systems under consideration are cold atoms in optical lattices. Therefore we give a short description of the systems and the realization of an "impure" optical lattice. Since from now on the tilt of the periodic lattice is not created by an electric field, a force $F$ is introduced which yields the external potential $Fx$.

## 3.1 The Gross-Pitaevskii equation

The wave function of a Bose-Einstein Condensate at low temperatures can be described by the Gross-Pitaevskii equation, which is a nonlinear Schrödinger equation. What follows is a short discussion on the Gross-Pitaevskii equation, see for instance [20]. We start with the Hamiltonian of a Bose-Einstein Condensate in a potential $V(\mathbf{r})$ in second quantization

$$H = \int d^3\mathbf{r}\, \hat{\Psi}^\dagger(\mathbf{r})\, H_0 \hat{\Psi}(\mathbf{r}) + \frac{1}{2} \int d^3\mathbf{r} \int d^3\mathbf{r}'\, \hat{\Psi}^\dagger(\mathbf{r}) \hat{\Psi}^\dagger(\mathbf{r}') V_{int}(\mathbf{r}, \mathbf{r}') \hat{\Psi}(\mathbf{r}') \hat{\Psi}(\mathbf{r}) \tag{3.1}$$

where $H_0 = -\hbar^2/2m\,\nabla^2 + V_{ext}$ is the single particle Hamiltonian with $m$ being the mass of the particle and $V_{ext}$ being the external potential acting on the system. $V_{int}(\mathbf{r}, \mathbf{r}')$ is the interaction between two particles, three or more body interactions are already neglected. $\hat{\Psi}(\mathbf{r})$ and $\hat{\Psi}^\dagger(\mathbf{r})$ are bosonic annihilation and creation operators of a boson at position $\mathbf{r}$ respectively, satisfying the following bosonic commutation rules

$$\left[\hat{\Psi}(\mathbf{r}'), \hat{\Psi}^\dagger(\mathbf{r})\right] = \delta(\mathbf{r}' - \mathbf{r}) \tag{3.2}$$

$$\left[\hat{\Psi}(\mathbf{r}'), \hat{\Psi}(\mathbf{r})\right] = \left[\hat{\Psi}^\dagger(\mathbf{r}'), \hat{\Psi}^\dagger(\mathbf{r})\right] = 0\,. \tag{3.3}$$

We can simplify the interaction potential $V_{int}(\mathbf{r}, \mathbf{r}')$, considering that the Bose-Einstein Condensate is a dilute and ultracold gas. Therefore we can neglect partial waves with an angular momentum $l \neq 0$. The interactions between atoms are then readily described using only s-wave collisions. To model this interaction, which is an elastic collision the following pseudo-potential is used

$$V_{int}(\mathbf{r}, \mathbf{r}') = \frac{4\pi\hbar^2 a_s}{m}\delta(\mathbf{r} - \mathbf{r}') = \bar{g}\delta(\mathbf{r} - \mathbf{r}')\,, \tag{3.4}$$

where $a_s$ is the s-wave scattering length. We use this pseudo-potential in Eq. (3.1) and integrate over $d^3\mathbf{r}$, which leads us to

$$H = \int d^3\mathbf{r}\, \hat{\Psi}^\dagger(\mathbf{r})\, H_0 \hat{\Psi}(\mathbf{r}) + \frac{\bar{g}}{2}\int d^3\mathbf{r}\, \hat{\Psi}^\dagger(\mathbf{r})\hat{\Psi}^\dagger(\mathbf{r})\hat{\Psi}(\mathbf{r})\hat{\Psi}(\mathbf{r})\,. \tag{3.5}$$

Together with the commutation rules Eq. (3.2) the Heisenberg equation of motion becomes

$$i\hbar\partial_t \hat{\Psi}(\mathbf{r}') = \left[H_0 + \bar{g}\hat{\Psi}^\dagger(\mathbf{r}')\hat{\Psi}(\mathbf{r}')\right]\hat{\Psi}(\mathbf{r}')\,. \tag{3.6}$$

Bogoliubov [21] proposed the following ansatz for solving Eq. (3.6), namely the decomposition of the field operator $\hat{\Psi}(\mathbf{r}')$ into a mean-field term (c-number) and a fluctuation term (operator)

$$\hat{\Psi}(\mathbf{r}') = \hat{a}_0\psi(\mathbf{r}') + \sum_m \hat{a}_m\psi_m(\mathbf{r}') \tag{3.7}$$

$$\approx \sqrt{N}\psi_0(\mathbf{r}') + \delta\hat{\Psi}(\mathbf{r}')\,, \tag{3.8}$$

where $\hat{a}_m$ is a bosonic annihilation operator and $N \gg 1$ is the occupation number of the state $\psi_0$, with $\|\psi_0\|^2 = 1$. The wave function could also have the norm $\|\psi_0\|^2 = N$, however the choice throughout this work is the former one. We now can use Eq. (3.7) in Eq. (3.6) and arrive to the time dependent Gross-Pitaevskii equation

$$i\hbar\partial_t\psi_0(\mathbf{r}, \mathbf{t}) = \left[H_0 + g|\psi_0(\mathbf{r}, \mathbf{t})|^2\right]\psi_0(\mathbf{r}, \mathbf{t})\,, \tag{3.9}$$

with the interaction given by

$$g = \bar{g}N = \frac{4\pi\hbar^2 a_s N}{m}\,. \tag{3.10}$$

During this derivation we neglected many body interactions and approximated the two body interaction with the pseudo potential in Eq. (3.4). We also

replaced the bosonic field operators with a wave function, by neglecting the fluctuations $\delta\hat{\Psi}(\mathbf{r}')$. These approximations are all valid, if the temperature is much lower than the transition temperature for the onset of the condensation and if the density of the condensate is also low enough (weakly-interacting system).

## 3.2 The one dimensional Gross-Pitaevskii equation

The purpose of this section is to obtain some understanding of the one-dimensional Gross-Pitaevskii equation, and especially the role of the nonlinear term in it. To start we need to know that a Bose-Einstein Condensate is produced by cooling a dilute gas in a harmonic trap

$$V(\mathbf{r}) = \frac{m}{2}\left(\omega_x^2 x^2 + \omega_y^2 y^2 + \omega_z^2 z^2\right) \tag{3.11}$$

below the transition temperature for the onset of condensation. In order to arrive at a quasi one-dimensional or two-dimensional Bose-Einstein Condensate, the trap has to be a very anisotropic one, to restrict the movement of the atoms in one or two dimensions. The atoms then only can populate the ground state of the harmonic potential. Since in this thesis only one-dimensional systems are considered it is necessary to get an effective interaction constant $g_{1D}$ for the one-dimensional case. For an anisotropic radially symmetric trap with $\omega_x \ll \omega_y = \omega_z = \omega_r$ and an interaction energy $g\rho_{max} \ll \hbar\omega_r$, where $\rho_{max}$ is the maximum density of the condensate, the condensate is in the ground state of the radial potential. This allows us to separate the field operator

$$\hat{\Psi}(\mathbf{r}) = \hat{\Psi}(x)\varphi(y,z) \tag{3.12}$$

into a one-dimensional field operator $\hat{\Psi}(x)$ and the ground state wave function $\varphi(y,z)$ of the two-dimensional harmonic oscillator

$$\varphi(y,z) = \frac{1}{\sqrt{\pi}a_\perp}\, e^{\left(-\frac{y^2+z^2}{2a_\perp^2}\right)}, \tag{3.13}$$

with $a_\perp^2 = \hbar/(m\omega_r)$. Using this decomposition for the interaction term (second one) in Eq. (3.1) leads to

$$H_{int} = \frac{\tilde{g}}{2}\int d^3\,\hat{\Psi}^\dagger(\mathbf{r})\hat{\Psi}^\dagger(\mathbf{r})\hat{\Psi}(\mathbf{r})\hat{\Psi}(\mathbf{r}) \tag{3.14}$$

$$= \frac{\tilde{g}}{2}\int dx\,\hat{\Psi}^\dagger(x)\hat{\Psi}^\dagger(x)\hat{\Psi}(x)\hat{\Psi}(x)\int dy\,dy\,|\varphi(y,z)|^4 \tag{3.15}$$

$$= \frac{\tilde{g}}{2\,2\pi a_\perp^2}\int dx\,\hat{\Psi}^\dagger(x)\hat{\Psi}^\dagger(x)\hat{\Psi}(x)\hat{\Psi}(x)\,. \tag{3.16}$$

As above, the ansatz Eq. (3.7) is made, $\hat{\Psi}(x) \approx \sqrt{N}\psi(x)$, with $\|\psi(x)\|^2 = 1$. This leads to the one-dimensional Gross-Pitaevskii equation

$$i\hbar\partial_t\psi(x,t) = \left[-\frac{\hbar^2}{2m}\nabla^2 + V(x) + g_{1D}|\psi(x,t)|^2\right]\psi(x,t)\,, \tag{3.17}$$

with the effective one-dimensional interaction constant

$$g_{1D} = \frac{g_{3D}}{2\pi a_\perp^2} = \frac{2\hbar a_s N}{m a_\perp^2}\,. \tag{3.18}$$

## 3.3 The optical lattice

An optical lattice is created by the interaction of light with matter. The energy states of an atom interacting with light are dependent on the intensity of the light, a spatially dependent intensity therefore leads to a spatially dependent potential energy. The simplest realization of an optical lattice is created by using two counter propagating laser beams, which produce a standing wave with a lattice period $\lambda_L/2$ where $\lambda_L$ is the wavelength of the laser. The periodic potential acting on the cold atoms in the laser field arises from the dipole force. The review [22] gives a good overview of the experimental realization of an optical lattice. We give a short description how the optical lattice is created, using a two state system as also done in [23]. $|g\rangle$ and $|e\rangle$ will be the ground-state and exited-state of the two state system. The electric field acting on an atom, which is small compared to the wavelength of the monochromatic laser is of the form

$$\mathbf{E}(\mathbf{r},t) = \mathbf{E}(\mathbf{r})\cos(\omega_L t)\,. \tag{3.19}$$

In this electric dipole approximation the Hamiltonian $H_{AF}$, which describes the interaction of the atom with the external field becomes

$$H_{AF} = -\mathbf{d} \cdot \mathbf{E}(\mathbf{r}, t)\,, \tag{3.20}$$

where $\mathbf{d} = d\hat{e}(|e\rangle\langle g| + |g\rangle\langle e|)$ is the dipole moment of the atom and $\hat{e}$ is the unit vector in the direction of quantization. Using Eq. (3.20) and the rotating wave approximation, we then can write the interaction energy as

$$H_{AF} = -\langle g|\,\mathbf{d}\cdot\mathbf{E}(\mathbf{r},t)\,|e\rangle\,|g\rangle\langle e| - \langle e|\,\mathbf{d}\cdot\mathbf{E}(\mathbf{r},t)\,|g\rangle\,|e\rangle\langle g| \tag{3.21}$$

$$\approx -\frac{1}{2}e^{i\omega_L t}\langle g|\,\mathbf{d}\cdot\mathbf{E}(\mathbf{r})\,|e\rangle\,|g\rangle\langle e| - \frac{1}{2}e^{-i\omega_L t}\langle e|\,\mathbf{d}\cdot\mathbf{E}(\mathbf{r})\,|g\rangle\,|e\rangle\langle g|\,. \tag{3.22}$$

The rotating wave approximation is valid if the electric field is close to resonance with the atomic transition frequency $\omega_0$. We then have $\Delta' = \omega_0 - \omega_L \ll \omega_0 + \omega_L$, where $\Delta'$ is called detuning. The rotating wave approximation now neglects the frequencies $\omega_0 + \omega_L$, which only would lead to fast oscillating terms in Eq. (3.21), rapidly averaging out. In the end the only relevant frequency is the detuning $\Delta'$ of the laser. The Hamiltonian describing the whole system of an atom interacting with the electric field is given by

$$H = H_A + H_{AF}\,, \tag{3.23}$$

where $H_A = \hat{p}^2/2m + \hbar\omega_0\,|e\rangle\langle e|$ is the atomic Hamiltonian. In matrix representation we can write Eq. (3.23) as

$$H = \hbar\omega_0\begin{pmatrix}1 & 0\\ 0 & 0\end{pmatrix} + \frac{\hat{p}^2}{2m}\begin{pmatrix}1 & 0\\ 0 & 1\end{pmatrix} - \frac{1}{2}\hbar\Omega(r)\begin{pmatrix}0 & e^{-i\omega_L t}\\ e^{i\omega_L t} & 0\end{pmatrix}, \tag{3.24}$$

where the Rabi frequency $\Omega(r)$ is given by

$$\Omega(r) = \Omega(r)^\dagger = \frac{\langle g|\,\mathbf{d}\cdot\mathbf{E}(\mathbf{r})\,|e\rangle}{\hbar} \approx \frac{\langle g|\,\mathbf{d}\,|e\rangle\cdot\mathbf{E}(\mathbf{r})}{\hbar}\,. \tag{3.25}$$

With the wave function

$$|\psi\rangle = \begin{pmatrix}e^{-i\omega_L t}\psi_e(\mathbf{r},t)\\ \psi_g(\mathbf{r},t)\end{pmatrix} = e^{-i\omega_L t}\psi_e(\mathbf{r},t)\,|e\rangle + \psi_g(\mathbf{r},t)\,|g\rangle \tag{3.26}$$

and Eq. (3.24) we gain the following two coupled Schrödinger equations

$$i\hbar\partial_t\psi_e(\mathbf{r},t) = \frac{\hat{p}^2}{2m}\psi_e(\mathbf{r},t) + \hbar\Delta'\psi_e(\mathbf{r},t) - \frac{\hbar\Omega(r)}{2}\psi_g(\mathbf{r},t) \tag{3.27}$$

$$i\hbar\partial_t\psi_g(\mathbf{r},t) = \frac{\hat{p}^2}{2m}\psi_g(\mathbf{r},t) - \frac{\hbar\Omega(r)}{2}\psi_e(\mathbf{r},t)\,. \tag{3.28}$$

Now to simplify the coupled equations Eq. (3.27) and Eq. (3.28), we use an approximation called adiabatic elimination. This approximation allows us to eliminate the variable which changes faster with time and to obtain an effective equation for the slowly varying variable. In this case this is done by assuming that $\hbar\Delta'$ is much larger than the kinetic energy of the atom. The elimination of the rapidly changing variable in Eq. (3.27) leads to $\psi_e \approx \frac{\Omega}{2\Delta'}\psi_g$. Then we can write Eq. (3.28), the Schrödinger equation for a particle in the ground state $|g\rangle$ as

$$i\hbar\partial_t\psi_g(\mathbf{r},t) = \left[\frac{\hat{p}^2}{2m} - \frac{\hbar\Omega(r)^2}{4\Delta'}\right]\psi_g(\mathbf{r},t)\,. \tag{3.29}$$

Meaning that the atom is moving in a dipole potential

$$V_{dipole} = -\frac{\hbar\Omega(r)^2}{4\Delta'}\,, \tag{3.30}$$

which is $\sim I(\mathbf{r})$, the intensity of the laser field. As mentioned in the beginning, two counter propagating lasers with wave number $k_L$ are used to generate a standing wave with an intensity of $I_0\cos^2(k_Lx)$; here only the one-dimensional case is considered. This leads to a periodic optical potential

$$V_{dipole} = \frac{\hbar\Omega(0)^2}{4\Delta}\cos^2(k_Lx)\,, \tag{3.31}$$

with a period $\lambda_L/2$.

Below, we give a short description of units used in experiments. Most of the time the Schrödinger equation under consideration here is the one-dimensional time dependent Schrödinger equation with an external homogeneous field given by

$$i\hbar\partial_t\psi(x,t) = \left[-\frac{\hbar^2}{2m}\frac{d^2}{dx^2} + \frac{V_0}{2}\cos(2k_Lx) + Fx\right]\psi(x,t)\,, \tag{3.32}$$

with $k_L$ being the wave number of the laser used to produce the optical lattice. The period of the created lattice is given by $a = \lambda_L/2$. If we use $k_L = 2\pi/\lambda_L$, we can write $k_L$ as $k_L = \pi/a$. In a next step we can rewrite Eq. (3.32) in dimensionless form, defining $z = k_Lx$. The natural unit of energy in these dimensionless units is the recoil energy $E_R = \hbar^2k_L^2/2m$, with one recoil energy

being the amount of kinetic energy an atom gains by absorbing a photon of a laser with wave number $k_L$. In these units Eq. (3.32) becomes

$$i\partial_\tau \psi(z,\tau) = \left[-\frac{d^2}{dz^2} + \frac{V_0}{2E_R}\cos(2z) + \frac{Fa}{E_R}\frac{z}{\pi}\right]\psi(z,\tau)\,, \tag{3.33}$$

where $V_0$ is the depth of the lattice in $E_R$. If gravity is the force $F$, $Fa/E_R$ can be evaluated as $Fa/E_R = m_{Rb}g\lambda_L/2E_R$, where $m_{Rb}$ is the mass of the ultracold Rubidium atoms and $g \approx 9.81 m/s^2$ is the acceleration of gravity. The units used in the numerical simulations are however chosen differently, because of their easy implementation in the numerical calculations, see App. A.1. These two choices of units have a one to one correspondence and can easily be converted into each other. As an example of the units described above, the band structure for an $10\,E_R$ deep optical lattice is shown in Fig. 3.1.

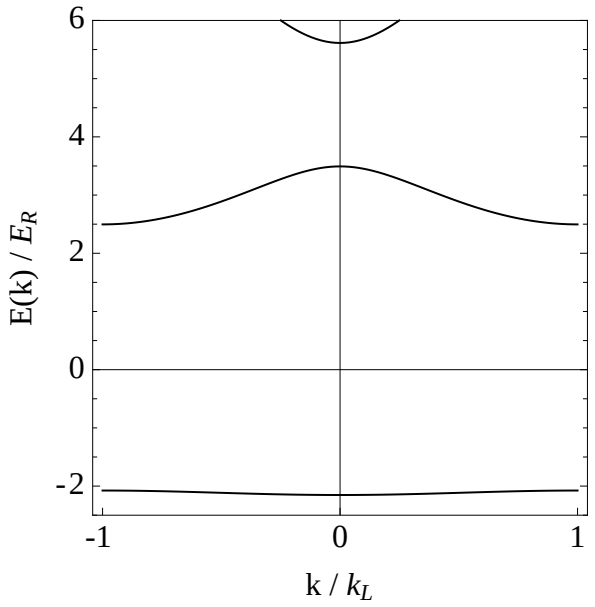


Figure 3.1: **Band structure for a $10\,E_R$ deep optical lattice.** A deep optical lattice has a very flat first band, $\Delta = 0.08\,E_R$. The gap between the first and second band $E_{gap} = 4.57\,E_R$ is fairly large.

## 3.4 Realization of disorder in an optical lattice

Ultracold atoms in optical lattices are extremely tunable quantum systems with the possibility of controlling the Hamiltonian of the system very easily.

In the main part of this thesis we will discuss disordered optical lattices as an extension to the perfect periodic optical lattice. Experimentally, disordered systems are an easy to realize extension to the the periodic case and we will give a short overview of the different kinds of possibilities to obtain a disordered optical lattice. A first approach to realize a disordered system uses speckle patterns [24]. Speckle patterns are created by laser light passing a diffusive platte, a device by which the incident light is scattered. The scattered laser light is interfering and creating the speckle pattern. The image of this pattern is shown onto the atoms and creates a disordered potential. We however, are not focusing on this technique, but consider the following two realizations of disorder. The first one is the realization of disorder by the bichromatic optical lattice [25]. The bichromatic lattice is created by a main lattice and an additional optical lattice with a different lattice constant an depth than the main lattice. This very controllable way of producing disorder is further described in Sec. 3.4.1. The second considered realization of disorder is the possibility of placing impurities on distinct lattice sites using a mixture of atoms. It is then possible to address a distinct lattice site in the optical lattice with an impurity [26]. This technique is further described in Sec. 3.4.2.

### 3.4.1 Disorder introduced by an incommensurate potential

In the case of disorder introduced by a bichromatic optical lattice, the potential in the Schrödinger equation is extended by an additional periodic potential:

$$V'(x) = V_0'(x) + V_1'(x) \tag{3.34}$$
$$= V_0' \cos(2k_{L_1}x) + V_1' \cos(2k_{L_2}x)\,, \tag{3.35}$$

where $k_{L_1}$ is the wave number of the laser producing the main lattice and $k_{L_2}$ is the wave number of the laser creating the second lattice acting as a perturbation to the first one. In the following we rewrite Eq. (3.35) in the units described in App. A.1, to use it in the numerical calculations

$$V(x) = V_0(x) + V_1(x) \tag{3.36}$$
$$= \cos(x) + s\,\cos(\alpha x)\,. \tag{3.37}$$

In Eq. (3.37) $\alpha$ is the fraction of the used laser's wave numbers and $s$ is the measure for the depth of the second lattice in terms of the first one. For $\alpha = p/q$ being a fraction of integers the potential is called quasi-periodic, for an irrational number $\alpha$, the potential is called incommensurate. The left part of

Fig. 3.2 shows the potentials $V_0(x)$ and $V_1(x)$ and the resulting incommensurate potential $V(x)$ for arbitrary values of $s$ and $\alpha$.

If the ratio $\alpha$ is the result of a fraction of two integers, the periodicity of the potential $V(x)$ is $2\pi q$. To ensure the incommensurability, this period has to be larger than the system size. We then can call the potential effectively incommensurate and it has the character of a disordered system.

### 3.4.2 Disorder introduced by an atomic mixture

Another possibility for introducing disorder in an optical lattice mimics the presence of impurity atoms in a crystal lattice. In an optical lattice this is done by a mixture of two different kinds of atoms. Atoms $A$, called scatterers occupy only some distinct wells of the optical lattice. The scatterers are now distributed over the lattice and act as random potentials to atoms of nature $B$ called test-particles, which move through the modified potential. The test-particles must not be trapped in the optical lattice. To ensure this, atoms $A$ and $B$ have to have different resonance frequencies in order that only atoms of species $A$ are trapped in the lattice.

The realization of this kind of disorder was accomplished in the numerical model, by adding a bump of Gaussian shape to the desired lattice site. See right of Fig. 3.2.

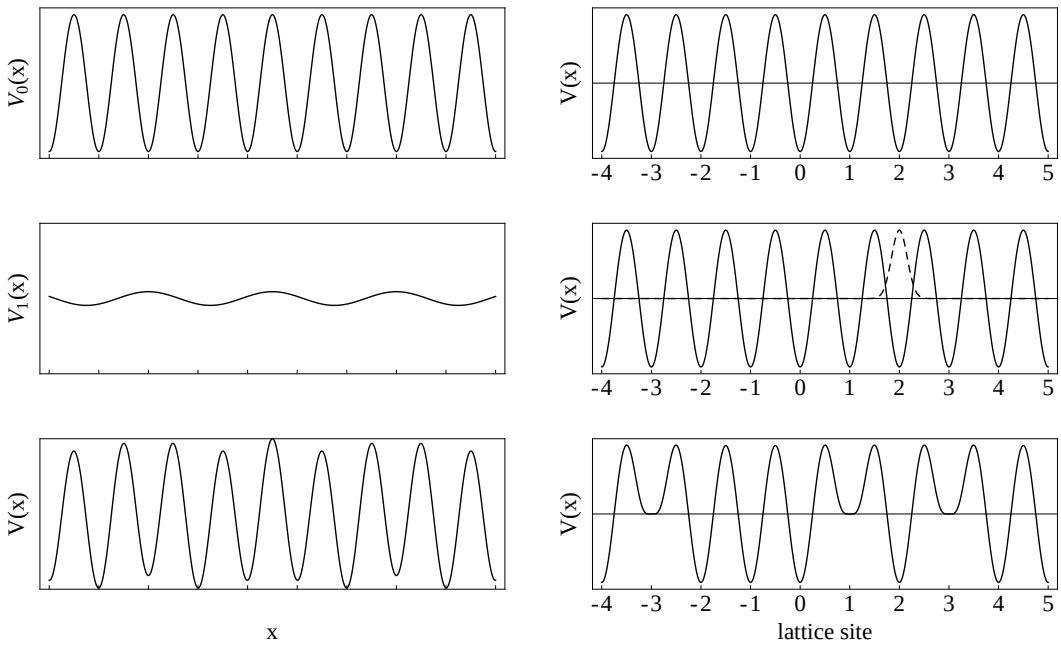


Figure 3.2: **Two kinds of realizations of disorder in an optical lattice.** Left panel: The top shows a sketch of the main lattice $V_0(x)$. In the middle the second lattice $V_1(x)$, which introduces the disorder is shown. On the bottom the whole bichromatic lattice $V(x)$, is illustrated. Right panel: On the top the main lattice $V(x) = \cos(x)$ is depicted. The plot in the middle illustrates the main lattice (solid line) and a bump of gaussian shape (dashed line) representing the impurity atom. On the bottom, the whole lattice with randomly placed impurities is shown.

# Chapter 4

# Numerical results

## 4.1 Bloch oscillations in optical lattices

We intend to solve the time dependent Schrödinger equation

$$i\,\hbar\,\partial_t\,\psi(x,t) = \left[-\frac{\hbar^2}{2}\nabla^2 + \cos(x) + F\,x\right]\psi(x,t)\,, \tag{4.1}$$

to investigate the time-evolution of the wave function. We solve Eq. (4.1) by means of the Split-Operator method [27]. This method entails the time-propagation of an initial wave function using a time-evolution operator. The time-evolution operator, which is proportional to $\exp((T+V)t)$, where $T$ and $V$ are the kinetic and potential energy of the Hamiltonian, can be split by using the Baker-Campbell-Hausdorff formula into a part containing only the kinetic energy and one containing only the potential energy, $\exp((T+V)t) \rightarrow \exp(Tt)\,\exp(Vt)$. The parts $\exp(Tt)$ and $\exp(Vt)$ are diagonal in momentum space and coordinate space, respectively. Starting with an initial wave function in coordinate space, a propagation by one time-step involves firstly a multiplication by $\exp(Vt)$, secondly a Fast-Fourier transform to momentum space, thirdly a multiplication by $\exp(Tt)$ and finally a Fast-Fourier transform back to coordinate space. A detailed explanation and an implementation of this method in *Mathematica* can be found in App. B.2. In App. A.1, the choice of units used in the numerical calculations throughout this thesis is described.

The initial wave packet is chosen to be a normalized Gaussian wave packet of the form

$$\psi_0(x,t=0) = \frac{1}{(2\,\pi\,\sigma^2)^{1/4}}\,e^{-\frac{x^2}{(2\,\sigma)^2}}\,. \tag{4.2}$$

Later in thesis we will also use the projection of the wave packet in Eq. (4.2) onto the first Bloch band as an initial state to describe the evolution only in

the lowest Bloch band, as described in Sec. 2.3. In the following the projected initial state is called $\psi_p(x, t = 0)$

$$|\psi_{p,n}\rangle = \int_{BZ} dk \, \langle \phi_{n,k}| \, |\psi_0\rangle \, |\phi_{n,k}\rangle \,, \tag{4.3}$$

where $\phi_{n,k}$ is the Bloch function for band $n$ and momentum $k$. Details are described in App. B.1.

These two different initial states should evolve differently in time. On the one hand, the wave packet $\psi_0(x, t = 0)$ has significant contributions from all the Bloch bands, which means that the evolution of $\psi_0(x, t = 0)$ in the system Eq. (4.1) should show a decay of the wave packet to higher bands due to Zener-tunneling. On the other hand, the wave packet $\psi_p(x, t = 0)$ should virtually show no decay to higher Bloch bands because it is entirely made out of the first Bloch band and the band gap separating the lowest Bloch band from the next one is fairly large.

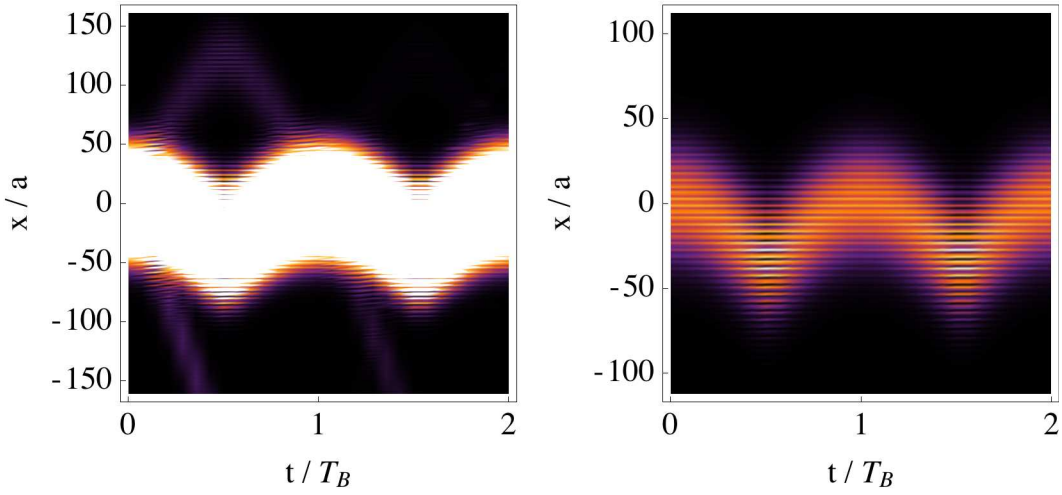


Figure 4.1: **Density $|\psi_0(x,t)|^2$ and $|\psi_p(x,t)|^2$ as a function of position and time.** The bright regions illustrate a high density, darker regions low density. On the left the wave packet $\psi_0(x, t)$ has contributions from all bands, therefore some weight is lost to the higher bands. On the right the time-evolution of the wave packet $\psi_p(x, t)$ shows no loss to higher bands because the wave function is entirely made out of the first Bloch band.

We choose the parameters for the numerical calculation in accordance with

the experimental situation in [5], which leads to a large amplitude of the Bloch oscillations. In this experiment the lattice depth is $1.4\,E_R$ leading to a scaled Planck constant $\hbar = 3.3806$. The field strength is set to $F = 0.005$. For both wave packets, the width $\sigma = 40\,\pi$, which means that initially 20 wells of the optical lattice are populated.

Fig. 4.1 summarizes the results of the propagation of $\psi_0$ and $\psi_p$ in time. The figure shows a density plot of $|\psi_0(x,t)|^2$ on the left and $|\psi_p(x,t)|^2$ on the right, with bright regions illustrating a high density, darker regions a low density. In the case of $\psi_0$ one can clearly see one part of the wave packet escaping to $-\infty$, which corresponds to the part of the wave packet that immediately tunnels through all the upper bands. The main part of the wave packet oscillates in the negative $x$-direction, with $T_B$ being the period of the oscillation. A third part of the wave packet oscillates with a larger amplitude than the main part in the positive $x$-direction. This oscillation can be thought of as part of the wave packet oscillating in the second band, which has a larger bandwidth and opposite curvature compared to the first band, leading to a larger amplitude and opposite velocity for the oscillation. The time-evolution of $\psi_p$ shows an evolution of the wave packet only in the first band, and no noticeable decay to upper bands, as expected.

## 4.2 Disorder in optical lattices introduced by an additional potential

We add a second periodic potential $V_{dis}(x)$ to the Hamiltonian in Eq. (4.1), in order to study the influence of disorder in an optical lattice on the Bloch oscillations

$$i\,\hbar\,\partial_t\,\psi(x,t) = \left[-\frac{\hbar^2}{2}\nabla^2 + \cos(x) + s\cos(\alpha\,x) + F\,x\right]\psi(x,t)\,. \tag{4.4}$$

We choose the values of the parameters together with Dominik Schneble to be realistic ones for the system in his lab at Stony Brook. In the following the lattice depth is taken to be $10\,E_R$ and the tilt of the lattice is given by $0.2\,g$ where $g = 9.81\,m/s^2$ is the acceleration of gravity. In scaled units this corresponds to $\hbar = 1.2649$ and $F = 0.0036$. The calculation of the band structure yields a width of the first band $\Delta = 0.0153$, which leads according to Eq. (2.34) to an amplitude of the Bloch oscillations $A_{BO} = 0.68\,a$, for the case of $s = 0$. The initial wave function is taken to be the one projected onto the first Bloch band of the system Eq. (4.4) with $s = F = 0$.

We first show the results of a numerical calculation where $s = 0$, leading

to undamped Bloch oscillations. Fig. 4.2 shows the average position $\langle x(t)\rangle = \int dx\, \psi^*(x)\, x\, \psi(x)$ of the Bloch oscillations with $\hbar = 1.2649$ and $F = 0.0036$. The undamped Bloch oscillations are clearly visible.

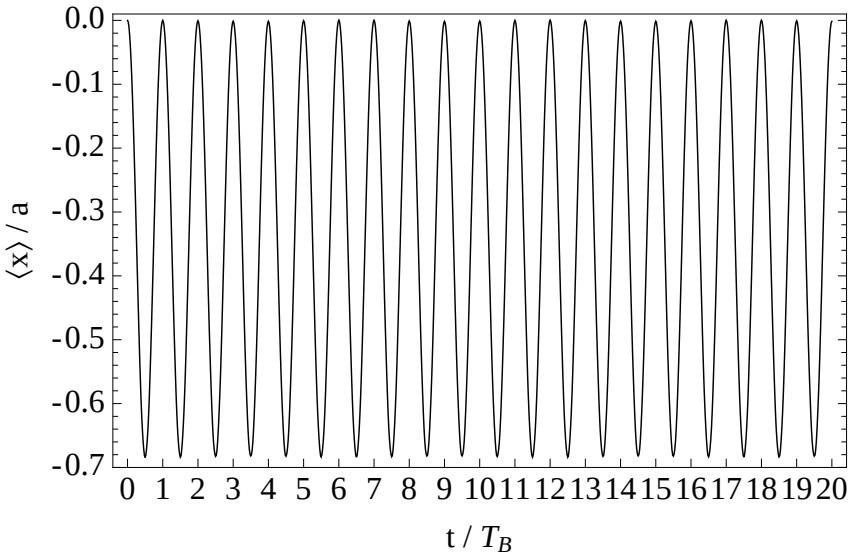


Figure 4.2: **Undamped Bloch oscillations.** Shown is the average position as a function of time for a tilted periodic lattice.

As described in Sec. 3.4.1, the addition of a second periodic potential is a model for a disordered optical system and is easy to implement experimentally as well as in the numerical calculation. The two parameters describing the disorder are $s$ and $\alpha$. In the following we will explore the effect of tuning these parameters on the Bloch oscillations. Two cases are then of interest:

- Changing the ratio $\alpha$ and keeping the amplitude of the disorder $s$ fixed.
- Keeping the ratio $\alpha$ fixed and varying the amplitude of the disorder $s$.

### 4.2.1 Changing the ratio $\alpha$ between the two optical lattices

In the following we keep the amplitude of the second optical lattice constant at $s = 0.0005$ and vary the ratio $\alpha$ of the two lasers producing the optical lattice from 0 to 2. To get an impression of how this kind of disorder affects the Bloch oscillations, the average position $\langle x(t)\rangle$ for the case $s = 0.0005$ and $\alpha = 0.4$ is shown in Fig. 4.3, to compare with Fig. 4.2.

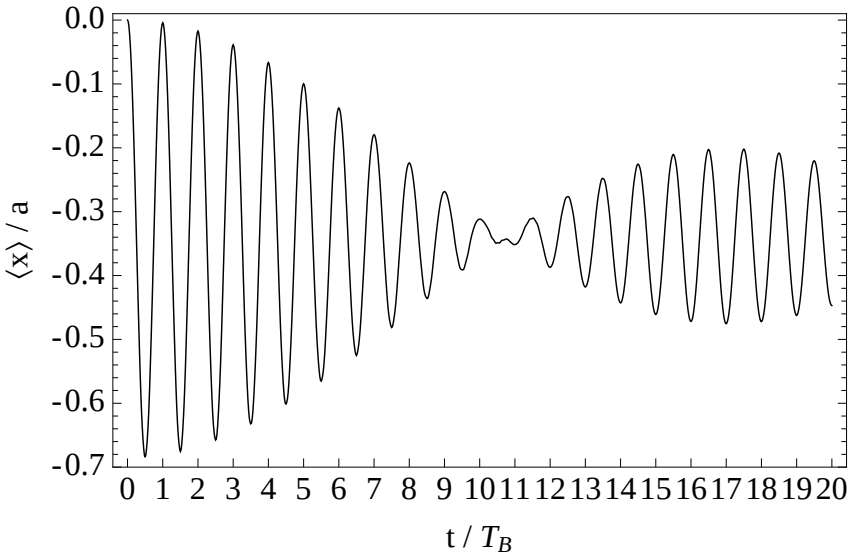


Figure 4.3: **Damped Bloch oscillations.** Shown is the average position as a function of time. In comparison to Fig. 4.2 the system is now a disordered one with $s = 0.0005$ and $\alpha = 0.4$ describing the disorder.

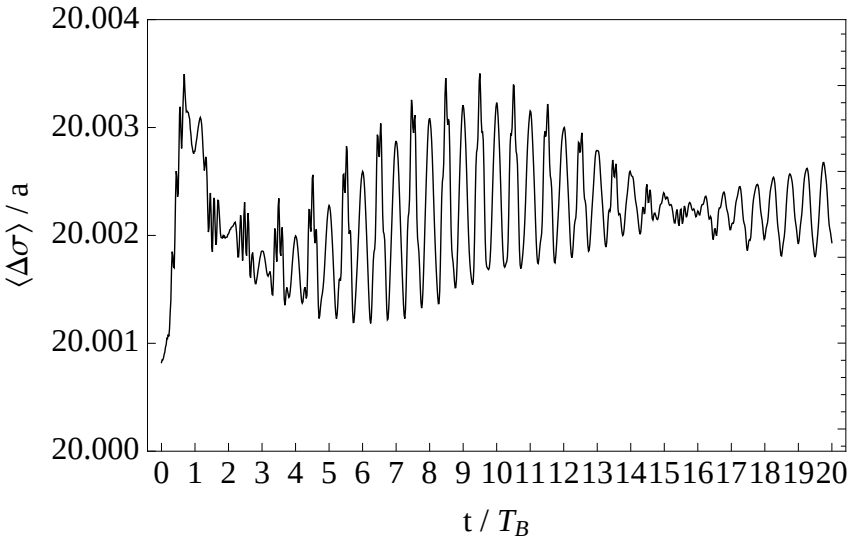


Figure 4.4: **Mean width $\Delta\sigma$ of a wave packetin a disordered system.** The wave packet starts to breath as it gets damped. The parameters for the disorder are the same as in Fig. 4.3.

One can clearly see the damping of the oscillations and also a revival of the oscillations after they have been damped completely. This revival is not a surprising observation because there are no dissipative processes present, in the numerical simulation as well as in the experimental optical lattice.

To illustrate that the energy is conserved in the system at the point where the wave packet is coming to rest (in Fig. 4.3 approximately at $t = 11\,T_B$), we also calculate the mean width of the wave packet in the following way, $\langle \Delta\sigma \rangle = \left( \langle x^2 \rangle - \langle x \rangle^2 \right)^{1/2}$, and show it for $\alpha = 0.4$ in Fig. 4.4.

One can see that the width of the wave packet has a maximum value at the time where the wave packet is at rest. As soon as the wave packet starts to move again, the width of the wave packet decreases. To summarize energy is exchanged between the center-of-mass motion and the breathing mode of the wave packet. An analogy would be a pendulum where the energy is oscillating between kinetic and potential energy. The properties of a breathing wave packet under the influence of the nonlinearity $g$ in the Gross-Pitaevskii equation in an optical lattice has been studied in [28] and [29].

The goal is now to establish a connection between the damping of the oscillations and the ratio $\alpha$. Therefore we simulate the time evolution of the system Eq. (4.4) for different values of $\alpha$. We again calculate the average position $\langle x(t, \alpha) \rangle$ and fit it to a function of the form

$$f\,(A, \eta, B; t) = A\, e^{-\eta\, t^2}\, \cos\left( \frac{2\pi}{T_B}\, t \right) - B \tag{4.5}$$

with $A$, $\eta$ and $B$ being fit parameters. The values for $\eta$ are then a measure of the damping of the oscillations. Fig. 4.5 summarizes the results of the simulation and shows $\eta$ as a function of $\alpha$ for $s = 0.0005$.

What strikes first in Fig. 4.5, are the values for the quasi-periodic cases $\alpha = \{0,\, 0.5,\, 1,\, 1.5,\, 2\}$, where the damping of the Bloch oscillations is zero.

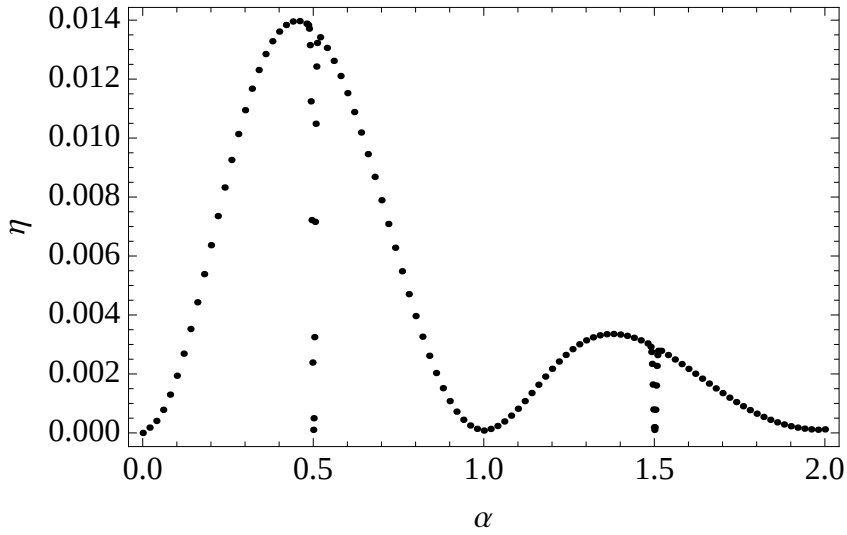


Figure 4.5: **Damping of Bloch oscillations as a function of $\alpha$ and $s = 0.0005$.** For five distinct values of $\alpha$ no damping is observed, which is explained in the text.

In the following we give an explanation for each of these points.

### $\alpha = 0$

In this case it is obvious that this corresponds to an offset in potential energy by $s$. The offset does not change the dynamics of the system and undamped Bloch oscillations are observed.

### $\alpha = 0.5$

To explain the situation $\alpha = 0.5$, one can think of a new system with a unit cell twice as large. The Brillouin zone of the new system is therefore half the size.

To illustrate what happens, we show on the right of Fig. 4.6 the band structure of a system with $s = 0.0005$ and $\alpha = 0.5$. In such a system, it follows from Eq. (2.33) that the Bloch period should be $1/2\,T_B$, where $T_B$ is the Bloch period for $s = 0$, in contrast to what can be seen on the left of Fig. 4.6. This leads to the conclusion that a large part of the wave function tunnels through the tiny gap at the edge of the new Brillouin zone to the upper band and fulfills the Bloch oscillation by tunneling back to the lower band at the other Brillouin zone boundary. Fig. 4.7 shows a scheme of the motion in the band picture to illustrate the explanation.

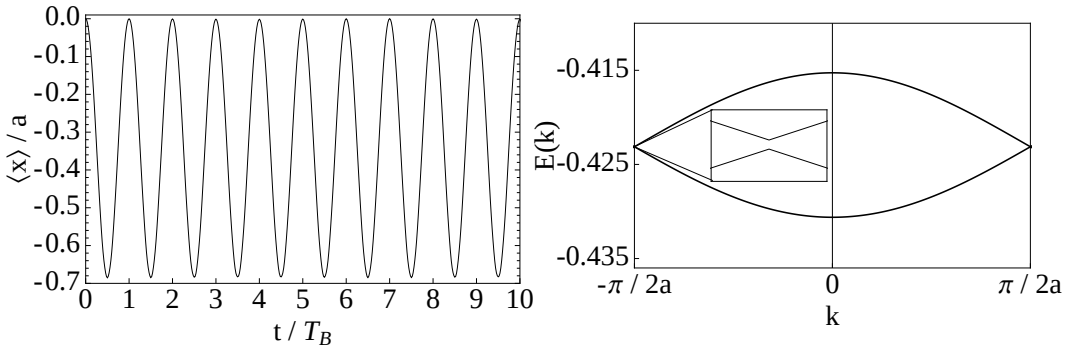


Figure 4.6: $\langle \boldsymbol{x(t)} \rangle$ **and band structure for** $\boldsymbol{\alpha = 0.5}$ **and** $\boldsymbol{s = 0.0005}$**.** On the left the average position is shown. Contrary to the expected bisection of $T_B$, it is still the same as if $s = 0$. The right shows the band structure. The Brillouin zone for a unit cell with two atoms ranges from $[-\pi/2a, \pi/2a]$. The inset shows a zoom in the region around the Brillouin zone edge where a gap opens due to a nonzero $s$.

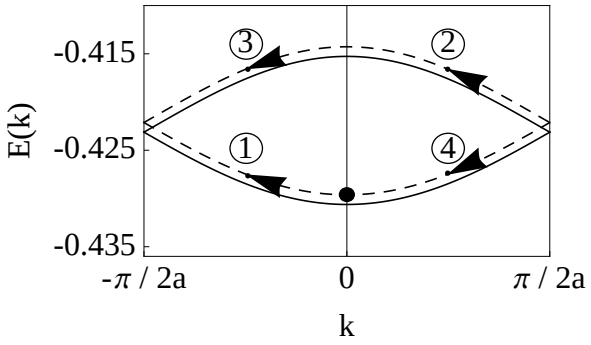


Figure 4.7: **Motion in a system with two periodic potential with** $\boldsymbol{s = 0.0005}$ **and** $\boldsymbol{\alpha = 0.5}$**.** This plot shows the motion in the band picture as described in the text.

The overlap of the wave function, $|\langle \psi(x, t = 0) | \psi(x, t) \rangle|$, gives even more insight. In Fig. 4.8 this overlap is plotted for the case $\alpha = 0.5$ and one can see that for late times a small peak develops at $(n + \frac{1}{2})T_B$, where $n$ is an integer. This means that the wave function, which was initially only built out of the first Bloch band of the system with $s = 0$, is slowly evolving into the system with the new periodicity of double the unit cell.

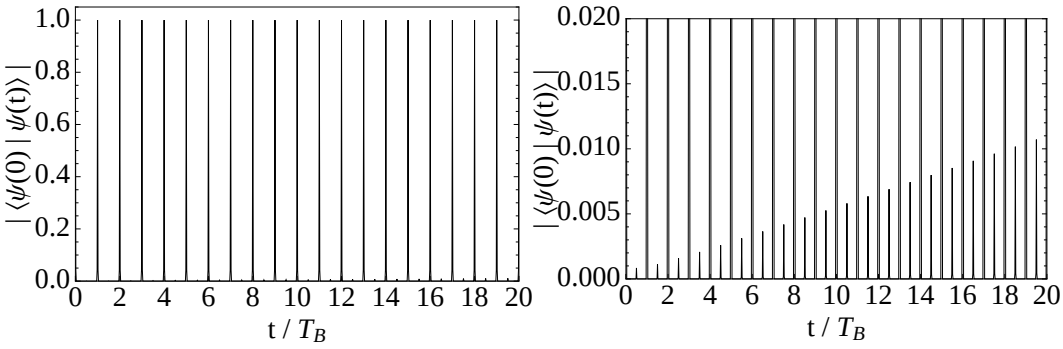


Figure 4.8: **Overlap $|\langle\psi(x,t=0)|\psi(x,t)\rangle|$ for $\alpha = 0.5$.** The left shows the overlap over the whole range. On the right a zoom is shown, which shows a small overlap developing at multiples of $1/2\,n\,T_B$.

### $\alpha = 1$

For $\alpha = 1$ the resulting potential has the period $a$, but with an amplitude $1 + s$, which leads to a modification of the bandwidth $\Delta$ and, according to Eq. (2.34), to a larger amplitude of the Bloch oscillations. Since $s \ll 1$ the change in the amplitude of the Bloch oscillations is not recognizable. Since the system is still a periodic one, the Bloch oscillations are undamped.

### $\alpha = 1.5$

In this case the explanation follows the one for $\alpha = 0.5$.

### $\alpha = 2$

The band structure for $\alpha = 2$ is not the same as in the case of $\alpha = 0$, because the Fourier components of these potentials are different. However, the periodicity for $\alpha = 2$ and $s \neq 0$ is still $a$. Therefore the Bloch oscillations are not damped by this potential.

From Fig. 4.5 arises also the question of weather the values $\alpha = 0.5$ and $\alpha = 1.5$ are singularities. To see the details in this regions, Fig. 4.9 therefore shows these regions enlarged. The plots reveal that the points $\alpha = 0.5$ and $\alpha = 1.5$ are not singularities, but we have a smooth function $\eta(\alpha)$.

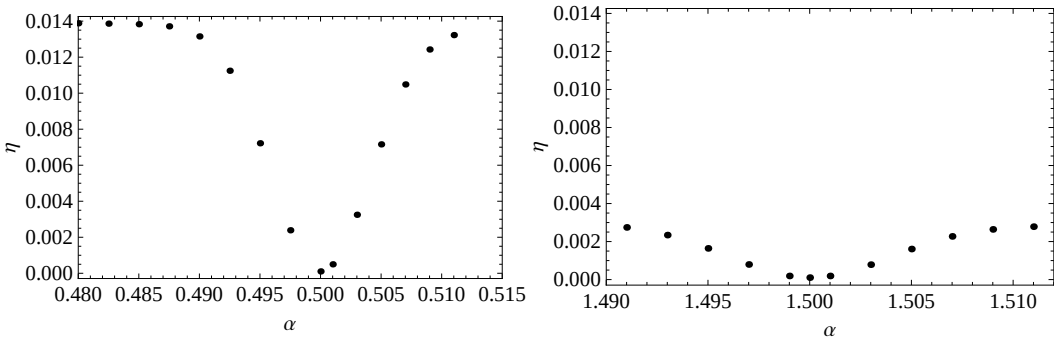


Figure 4.9: **The regions around $\alpha = 0.5$ and $\alpha = 1.5$ enlarged.** The zoom into these regions shows that $\eta$ is a smooth function of $\alpha$. Here $s = 0.0005$.

### 4.2.2 Changing the depth $V_0$ of the optical lattices

To further investigate the regions around $\alpha = 0.5$ and $\alpha = 1.5$, we now change the depth of the optical lattice to $V_0 = 1\,E_R$ (black), $V_0 = 5\,E_R$ (blue), $V_0 = 8\,E_R$ (orange) and $V_0 = 10\,E_R$ (red). The strength of the disorder is kept at $s = 0.0005$ in all cases. Tab. 4.1 gives an overview on the values of the scaled units and the resulting amplitude of the Bloch oscillations.

| $V_0\,/E_R$ | $\hbar$ | $F$ | $A_{BO}\,/a$ |
|---|---|---|---|
| 1 | 4 | 0.0357 | 6.90 |
| 5 | 1.7889 | 0.0071 | 2.36 |
| 8 | 1.4142 | 0.0045 | 1.10 |
| 10 | 1.2649 | 0.0036 | 0.68 |

Table 4.1: **Summary on amplitudes $A_{BO}$ for different lattice depths $V_0$.** A deeper lattice has shallower bands, the results are Bloch oscillations with smaller amplitudes.

The change in the depth of the lattice affects the amplitude of the Bloch oscillations as can be read in Tab. 4.1. For smaller lattice depths, the wave packet now moves over a larger range in coordinate space than before, and should therefore experience the disordered potential landscape in a more detailed way, since the width of the wave packet is left unchanged. As above, a fit to $\langle x(t)\rangle$ was performed according to Eq. (4.5).

The dependance of the damping on $\alpha$ for the different depth of the optical lattice is shown in Fig. 4.10. The first thing that can be seen from Fig. 4.10 is that the overall damping decreases as the depth of the lattice also decreases,

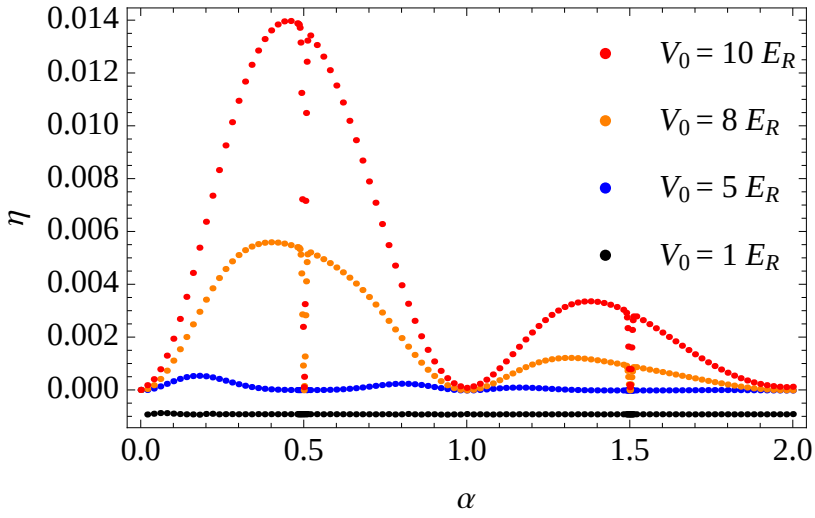


Figure 4.10: **Damping of Bloch oscillations for different depths of the optical lattice at $s = 0.0005$.** With a decreasing depth of the optical lattice, we also observe a decreasing damping of Bloch oscillations.

which is not a surprising effect. As a second effect one can see, that $\eta(\alpha)$ in the regions around $\alpha = 0.5$ and $\alpha = 1.5$ is no longer a fast changing function of $\alpha$. The explanation would be that the wave packet is now more sensitive to a change of the incommensurability parameter $\alpha$. To define how effectively incommensurate the potential is, the length scale on which the Bloch oscillations happen is a crucial parameter.

### 4.2.3 Changing the amplitude $s$ of the disorder potential

To increase the disorder the amplitude $s$ of the disorder potential has to be turned up. Intuitively more disorder should lead to a faster damping of the Bloch oscillations, which indeed can be seen in Fig. 4.11, where $\eta$ is again plotted over $\alpha$ for $s = 0.0005$ (black), $s = 0.001$ (blue) and $s = 0.0013$ (orange) at a fixed lattice depth of $10\,E_R$. One can clearly see the increased damping if the disorder is increased by turning up the parameter $s$. The shape of the $\alpha$-dependance stays the same for different values of $s$.

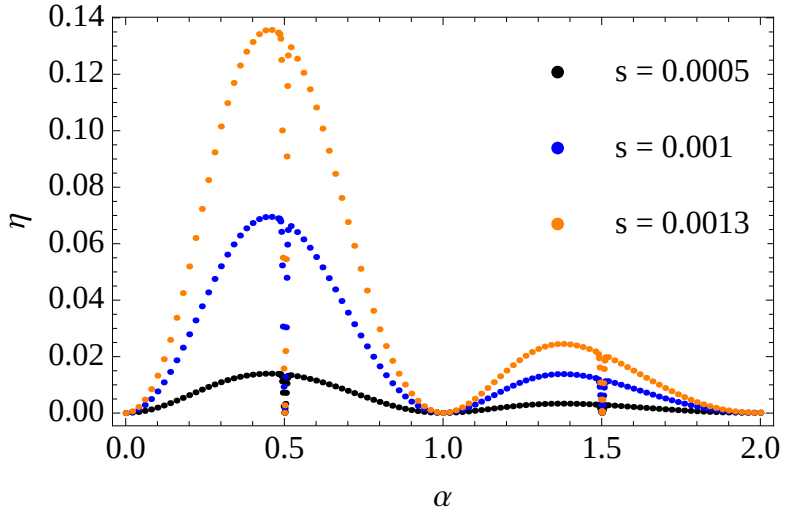


Figure 4.11: **Damping of Bloch oscillations for different disorder strengths *s*.** A larger amplitude $s$ leads to a faster damping of the Bloch oscillations, which leads to a larger $\eta$.

### 4.2.4 Analytical Approach

In order to help explain the damping of Bloch oscillations due to the disorder, we now try an analytical approach. This approach uses a tight binding model of the Schrödinger equation Eq. (4.4). We can write

$$i\hbar\partial_t\psi(x,t) = [H_0 + s\cos(\alpha x)]\,\psi(x,t)\,, \tag{4.6}$$

with $H_0$ defined as

$$H_0 = -\frac{\hbar^2}{2}\nabla^2 + \cos(x) + Fx\,. \tag{4.7}$$

This Hamiltonian has, as described in Sec. 2.4, stationary solutions in the form of Wannier-Stark states $\Psi_{\mu,n}$

$$H_0\Psi_{\mu,n} = \varepsilon_{\mu,n}\Psi_{\mu,n}\,, \tag{4.8}$$

where $\mu$ is the Wannier-Stark ladder index and $n$ the lattice site index. The eigen-energies of Eq. (4.8) build the Wannier-Stark ladder $\varepsilon_{\mu,n} = \varepsilon_{0,n} + 2\pi Fn$. In the following, the ladder index $\mu$ is suppressed because only the lowest ladder is taken into account due to negligible Zener tunneling. We obtain the necessary eigenstates of Eq. (4.8) by the above mentioned tight binding model in a site basis. In matrix form the Hamiltonian we have to diagonalize can be

written as

$$H_{0,nm} = J\left(\delta_{n-1,m} + \delta_{n+1,m}\right) + 2\pi nF\,\delta_{n,m}\,, \tag{4.9}$$

where $n$ is the lattice site index and $J$ is the hopping element. The hopping element is taken to be $J = \Delta/4$, where $\Delta$ is the bandwidth of the lowest Bloch band.

The wave function in Eq. (4.6) is now expanded in terms of the Wannier-Stark states $\Psi_n$

$$\psi(x,t) = \sum_m c_m(t)\Psi_m(x)\,, \tag{4.10}$$

with time dependent expansion coefficients $c_m(t)$. This leads to

$$i\hbar\partial_t \sum_m c_m(t)\Psi_m(x) = \sum_m (\varepsilon_0 + 2\pi Fm)c_m(t)\Psi_m(x) + \sum_m s\cos(\alpha x)c_m(t)\Psi_m(x)\,, \tag{4.11}$$

which we can multiply from the left by $\Psi_n^*(x)$ and integrate over all space. With the property

$$\int_{-\infty}^{\infty} dx\,\Psi_n^*(x)\Psi_m(x) = \delta_{n,m} \tag{4.12}$$

Eq. (4.11) becomes

$$i\hbar\partial_t c_n(t) = 2\pi Fnc_n(t) + s\sum_m c_m(t)\Psi_n^*(x)\cos(\alpha x)\Psi_m(x)\,, \tag{4.13}$$

where $\varepsilon_0$ would only lead to a global phase and has been set to zero without loss of generality. We now have to take a closer look at the last term in Eq. (4.13). Since the Wannier-Stark states are exponentially localized at a lattice site, we can safely neglect the overlap $\displaystyle\int_{-\infty}^{\infty} dx\,\Psi_n^*(x)\Psi_{n+1}(x)$ in this model. Therefore, we can write Eq. (4.13) as

$$i\hbar\partial_t c_n(t) = 2\pi Fnc_n(t) + sc_n(t)\cos(2\pi\alpha n)\,. \tag{4.14}$$

The next step is to split the time dependent expansion coefficients $c_n(t)$ into an amplitude and phase

$$c_n(t) = \rho_n(t)e^{i\varphi_n(t)}\,. \tag{4.15}$$

As an initial state to this problem the $c_n$ are of the form

$$c_n \sim e^{-\frac{n^2}{(2\sigma)^2}}\,. \tag{4.16}$$

Eq. (4.14) together with Eq. (4.15) leads us to

$$i\hbar\dot{\rho_n} - \hbar\dot{\varphi_n}\rho_n = 2\pi F n\rho_n + s\rho_n \cos(2\pi\alpha n)\,, \tag{4.17}$$

the dot denotes the derivative with respect to time. We assume a broad spread of the initial state, which leads to small amplitudes $\rho_n$, $\rho_n(t=0) \ll 1$. The amplitudes $\rho_n(t)$, compared to the phases $\varphi_n(t)$, are slowly changing in time, we therefore assume the amplitudes to be constant in time. We then write Eq. (4.17) as two differential equations

$$\hbar\dot{\varphi_n} = -2\pi F n - s\cos(2\pi\alpha n) \tag{4.18}$$

$$\hbar\dot{\rho_n} = 0\,, \tag{4.19}$$

with solutions

$$\varphi_n(t) = -\frac{1}{\hbar}\left(2\pi F n + s\cos(2\pi\alpha n)\right)t \tag{4.20}$$

$$\rho_n(t) = \rho_n(0)\,. \tag{4.21}$$

The normalized time independent $\rho_n$ are taken to be

$$\rho_n = \frac{1}{\sqrt{2\pi\sigma^2}} e^{-\frac{n^2}{(2\sigma)^2}}\,, \tag{4.22}$$

in order to be similar to the initial states used in the previous chapters.

### The tight binding model compared to exact numerical calculations

The wave function in the time dependent Schrödinger equation Eq. (4.6) can now be written as

$$\psi(x,t) = \sum_n c_n \Psi_n \tag{4.23}$$

$$= \sum_n \rho_n e^{-\frac{i}{\hbar}(2\pi F n + s\cos(2\pi\alpha n))t}\Psi_n\,. \tag{4.24}$$

We obtain the functions $\Psi_n$ via the simple tight binding Hamiltonian Eq. (4.9). In Fig. 4.12 the exact numerical result (dashed-red line) for the average position $\langle x(t)\rangle$ is compared to the one attained by using the above described model (solid black line). The parameters were in scaled units $\hbar = 1.2649$, $F = 0.0036$, $s = 0.0005$ and $\alpha = 0.4$.

It should be noted that this tight binding approximation is only in accordance with the exact calculation for values of $\alpha < 1$. However, this simple

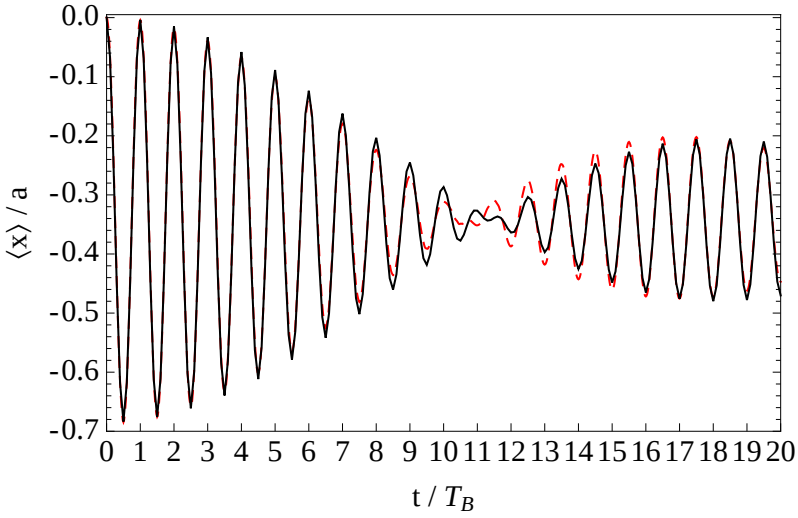


Figure 4.12: **Exact numerical results compared to a tight binding model.** The dashed-red line shows the result of an exact numerical simulation compared to the solid black line which shows the result attained by a tight binding model.

model allows us to gain at least some insight in the question why the Bloch oscillations are damped. We can see from Eq. (4.20) that the phase of the wave function no longer evolves linearly with time with a nonzero $s$. Later on in Sec. 4.4, we will have a closer look on the evolution of the wave packet in momentum space and see that this nonlinear evolution of the phase leads to a broadening of the momentum distribution in time, causing the damping of the Bloch oscillations.

## 4.3 Disorder introduced by impurities at distinct lattice sites

The goal in this section is to examine the influence of impurities at distinct lattice sites on Bloch oscillations. Therefore, we consider the following Hamiltonian

$$i\,\hbar\,\partial_t\,\psi(x,t) = \left[-\frac{\hbar^2}{2}\nabla^2 + \cos(x) + V_{imp}(x) + F\,x\right]\psi(x,t)\,, \tag{4.25}$$

where $V_{imp}(x)$, as described in Sec. 3.4.2, is a sum of Gaussians centered at a specific lattice site. The Gaussian itself has the form

$$V_{imp,n}(x) = e^{-\frac{(x-x_n)^2}{2\sigma_{imp}^2}}, \tag{4.26}$$

where $\sigma_{imp}$ is the width of the Gaussian and $x_n$ denotes the lattice site $n$ of its center. We chose a Gaussian to mimic an impurity in the lattice because it is a very controllable function and it is easy to implement in the numerical calculation. Throughout this section, the Gaussian has an amplitude equal to 1 and a width $\sigma_{imp} = 0.1\,\pi^2$, in order to cut off one well of the cosine potential. See the right of Fig. 3.2 for a schematic picture. The parameters for the system ($\hbar$ and $F$) in this section are chosen as in Sec. 4.1, in order to have a larger amplitude $A_{BO}$ of the Bloch oscillations. The initial wave function is of the form in Eq. (4.2).

### 4.3.1 Patterns of impurities

We first test if a periodic pattern of impurities will show Bloch oscillations, therefore we place an impurity on every second lattice site. This can be thought of as doubling the lattice constant; $a' = 2\,a$. This should lead to a halving of the Bloch time $T_B$, where throughout this section $T_B$ will be the reference Bloch time of the pure system with lattice constant $a$. The result of a simulation is shown in Fig. 4.13, where as before the average position of the wave packet is plotted over time. The plot is slightly distorted, because the initial wave function is not projected on a first band of the periodic impure system. Despite this fact, the plot shows exactly what is expected, a new period for the Bloch oscillations, namely $T_B/2$. Although the lattice is now impure, the Bloch oscillations still exist, because of the periodic placement of impurities. The size of the new unit cell is not restricted to be $2\,a$. In general, it could be $a' = l\,a$, with $l$ being an integer. This will lead to a Bloch time

$$T_{B,l} = \frac{2\pi\hbar}{laF}, \tag{4.27}$$

where $l$ is the size of the new unit cell. Summing up we can see that the introduction of a periodic pattern of impurities in a formerly clean system, does not destroy the Bloch oscillations. However, there is a constraint to the width of the initial wave packet. It has to be broad enough to cover at least one new unit cell in order to "experience" the new periodicity.

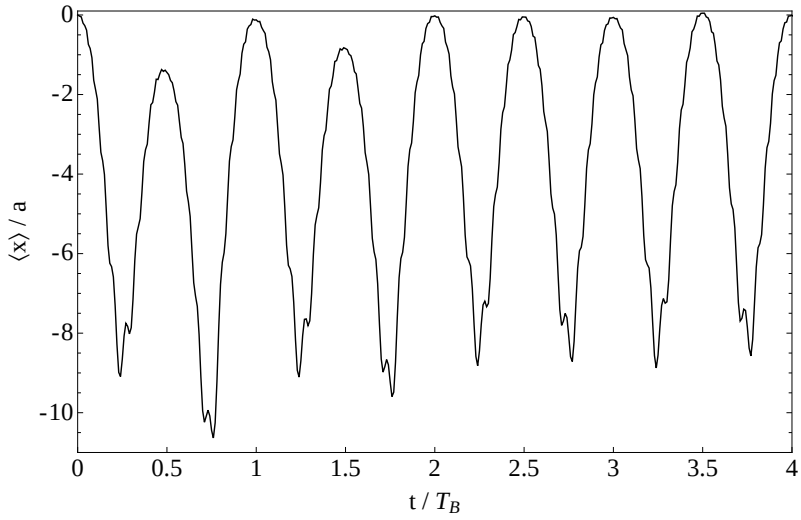


Figure 4.13: **Bloch oscillations in a system with an impurity on every other lattice site.** Placing an impurity on every other lattice site leads to a bisection of $T_B$ as anticipated from Eq. (2.33)

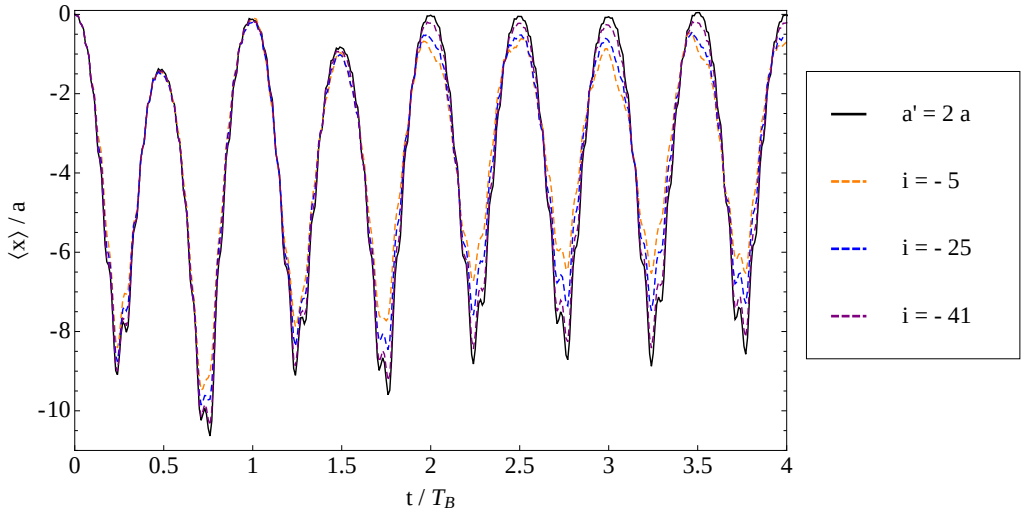


Figure 4.14: **Bloch oscillations in a system with a slightly periodic pattern of impurities.** An impurity is placed on every other lattice site except site $i$. The black solid line shows the case of an impurity on every second lattice site. Removing an impurity on site $i$ destroys the formerly periodic pattern and as a consequence the Bloch oscillations are damped.

It is now instructive to check if a slightly non-periodic placement of impurities affects the Bloch oscillations. Therefore, we place an impurity on every second site except lattice site $i$. The impurities are only removed in an interval between lattice site $-41$ to 21, because the wave packet only moves over this finite range on the lattice. In Fig. 4.14 we showe the results. We see that the Bloch oscillations are not destroyed completely by the non-periodic placement of impurities, but instead get damped in a way similar to that of Sec. 4.2. Removing an impurity from the periodic pattern on a site nearly out of the wave packet's range of movement causes less damping of the oscillations (compare the black and purple lines in Fig. 4.14). In conclusion we can say that even the slightest perturbation of the periodic pattern affects the Bloch oscillations, and as a consequence they get damped. In the next section the impurities are randomly placed in the lattice, and we will see that the influence on the Bloch oscillations is stronger.

### 4.3.2 Randomly distributed impurities

It is also very easy to introduce a totally random distribution of impurities in the system, and investigate the influence on Bloch oscillations. With the knowledge from above, the impurities are only placed on lattice sites in the interval $[-41, 21]$.

To get a first impression of how the randomly placed impurities affect the Bloch oscillations, we plot as in the sections before $\langle x(t) \rangle$. The result can be seen in Fig. 4.15. The number of impurities placed in lattice is chosen to be $1, 2, 3, 4, 5, 10$ and is shown in parts $a$) to $f$) of Fig. 4.15 respectively. The different colors denote different kinds of random placements of the impurities. The general trend with increasing disorder, is an increased damping of the Bloch oscillations, up to a point where no clear movement of the wave packet's center can be recognized. Looking at each part of Fig. 4.15 separately, one can see that how the Bloch oscillations are damped depends very much on the placement of the impurities, but due to the random placement, the damping of the Bloch oscillations happens in no distinct way.

In the case of random disorder, the overlap $|\langle \psi(x, t = 0) | \psi(x, t) \rangle|$ gives more insight into what happens with increasing disorder. Fig. 4.16 shows the overlap for the different amounts of disorder (again parts $a$) to $f$)). Illustrated dashed-red in each part is the overlap for the case of zero disorder, where the wave packet fully returns after each Bloch period. In comparison with the dashed-red line, the correlation of the wave function in a disorder system (solid black line) at multiples of $T_B$ decreases with increasing disorder. This leads to the conclusion, that randomly distributed impurities destroy the Bloch oscillations.

Here we can see an analogy to Anderson Localization [30]. Anderson Localization occurs in a randomly disordered metal with non-interacting electrons. The disorder induces a metal to insulator transition, or differently speaking a transition from extended states to localized states. Numerically the localization can be investigated in simple tight binding model, where the disorder is realized by randomly varying onsite energies. In the system we consider here, the randomly disordered optical lattice, we also observe a localization of the wave packet, if random disorder is introduced.

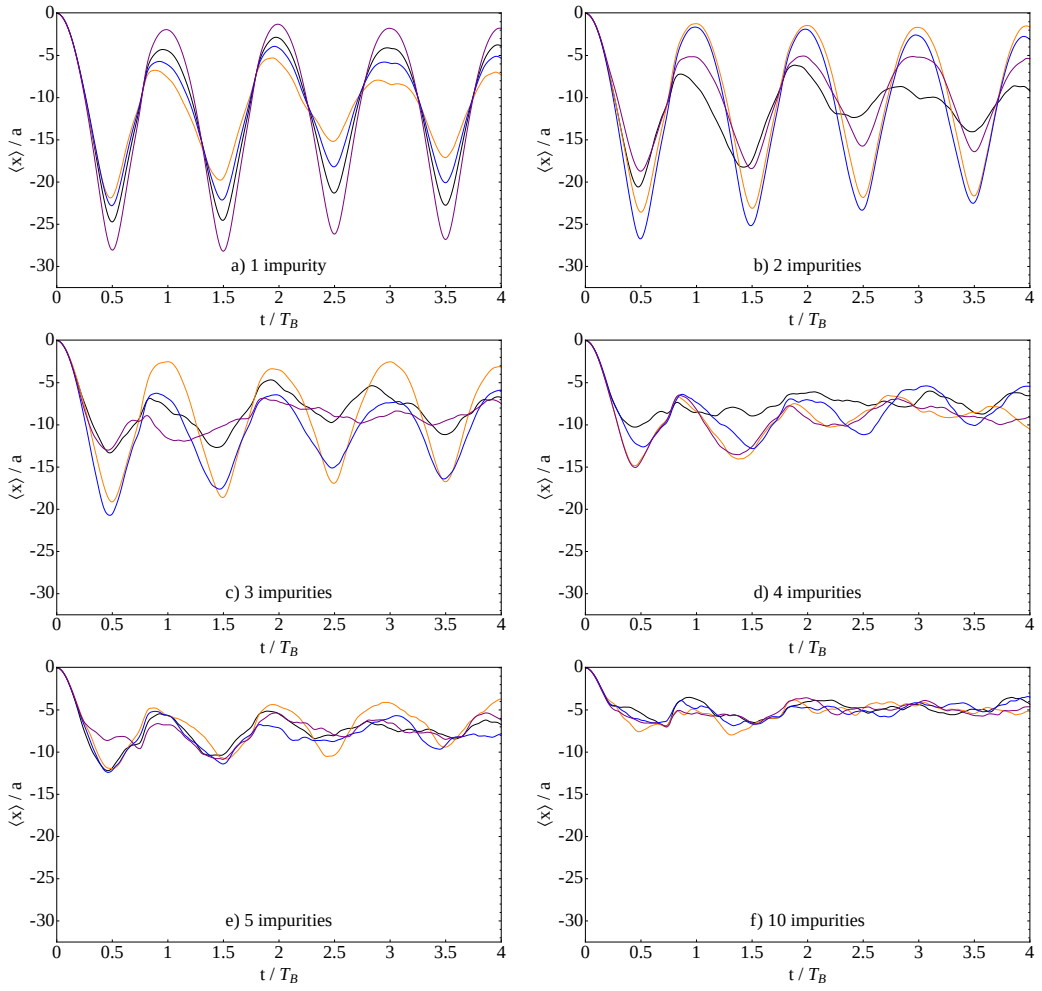


Figure 4.15: $\langle \mathbf{x} \rangle$ (**t**) **for randomly distributed impurities.** Parts $a$) to $f$) show for $1, 2, 3, 4, 5, 10$ impurities in the system the influence on the damping. Increasing the amount of disorder increases the damping of Bloch oscillations. The different colors in each part illustrate different configurations of random disorder.

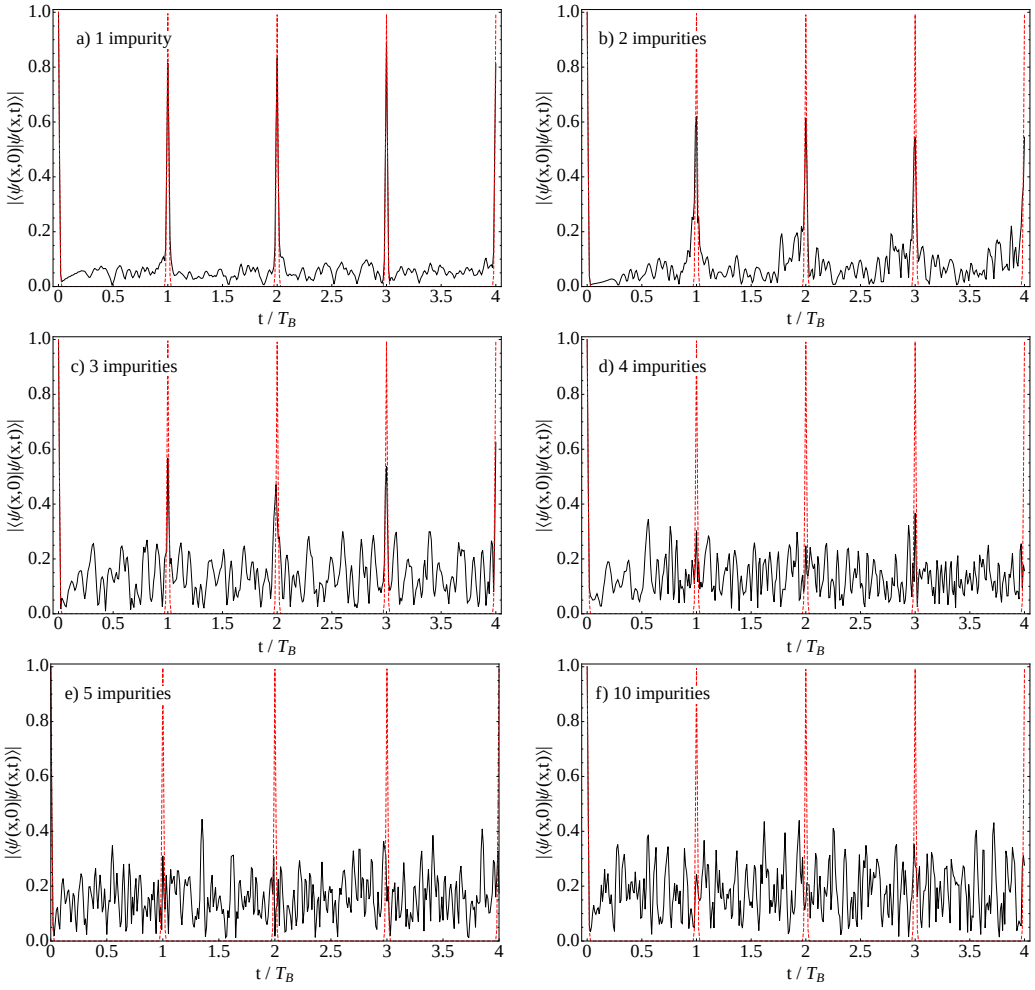


Figure 4.16: **Overlap of the wave function for the case of randomly distributed impurities.** For a random distribution of impurities the overlap $|\langle\psi(x,t=0)|\psi(x,t)\rangle|$ is shown (black) in comparison to the overlap of a pure system (dashed-red). With increasing disorder the wave packet does not return and the overlap at multiples of $T_B$ is less than 1, meaning no periodic movement of the wave packet is recognizable.

## 4.4 Mechanism of the damping

In an undisturbed tilted lattice, the energies differ from site to site by

$$\Delta E = a\, F\,, \tag{4.28}$$

where $F$ is the field that tilts the lattice and $a$ is the lattice constant. We can define a phase $\varphi(t)$ in the evolution of the wave function using Eq. (2.30) and Eq. (2.31) in the following way

$$\varphi(t) = \frac{Fa}{\hbar} t = \frac{\Delta E}{\hbar} t\,. \tag{4.29}$$

In the case of absent disorder the energy difference $\Delta E$, is the same from site to site. This leads to a constant evolution of the phase and momentum in time.

If disorder is introduced in the system, the energy difference $\Delta E$ from site to site is no longer a constant. The energy difference becomes a spatially dependent one, $\Delta E(x)$, leading to a varying phase and momentum evolution.

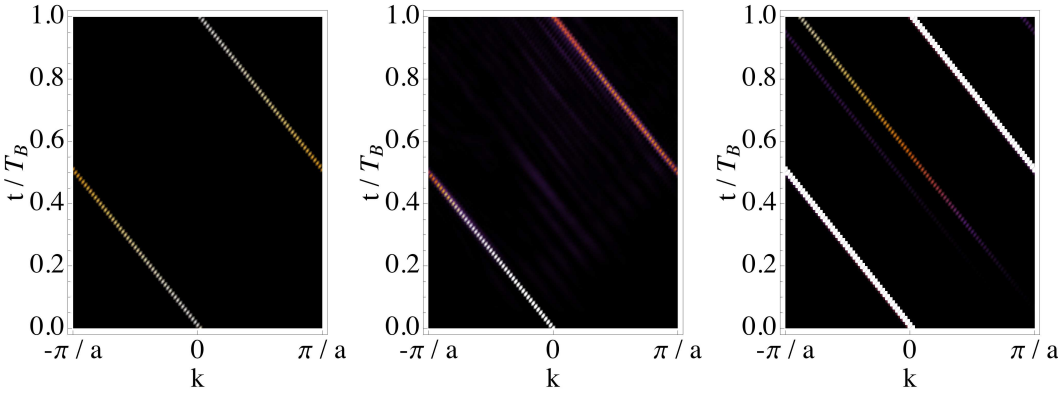


Figure 4.17: **Density $|\psi(k,t)|^2$ with and without disorder.** Left: If no disorder is present in the system, this will lead to a constant evolution of the momentum. Middle: The evolution of the momentum for 2 randomly placed impurities shows a weak secondary peaks and a broadening in the main peak of the momentum. Right: In the case of the bichromatic lattice distinct secondary peaks start to appear.

This can be observed in the time evolution of the momentum, which is shown in Fig. 4.17, as the density $|\psi(k,t)|^2$. The left plot in Fig. 4.17 shows the evolution of the momentum in the unperturbed case, where the narrow

momentum distribution evolves constantly in time. The plots in the middle and on the right illustrate the time evolution of the momentum for a random pattern of 2 impurities in the lattice and for the bichromatic lattice respectively. In the case of disorder, the momentum no longer evolves constantly, but we can see smaller peaks arising shortly after the beginning of the movement.

There is also a difference in the momentum evolution for the two different kinds of disorder, which we can also see in Fig. 4.17. In the case of a random distribution of impurities the arising peaks are still very low, but we can see a broadening of the main peak of the momentum distribution. The evolution of the momentum in the case of a bichromatic lattice shows no such broadening in the main peak, but very distinct and higher secondary peaks.

The broadening of the main peak and occurrence of secondary peaks in the momentum distribution causes the damping of the Bloch oscillations, since the momentum no longer evolves linearly with time.

## 4.5 Disorder and interaction

In this section the interplay between disorder and interaction, which is described in the full Gross-Pitaevskii equation Eq. (3.9) by the mean field term $g\,|\psi(x,t)|$, is investigated. It is known from [28, 29], that the interaction alone leads to a damping of the Bloch oscillations. To illustrate this effect we perform a numerical simulation of the following system

$$i\,\hbar\,\partial_t\,\psi(x,t) = \left(-\frac{\hbar^2}{2}\frac{d^2}{dx^2} + \cos(x) + Fx + g\,|\psi(x,t)|^2\right)\,\psi(x,t)\,. \tag{4.30}$$

To solve the full Gross-Pitaevskii equation with the Split-Operator Method, the wave function appearing in the mean-field term is taken to be the one from the last time-step. If the time-steps are small enough, the error will be negligible. The implementation in *Mathematica* is shown in App. B.3.

The interaction term $g$ in the Gross-Pitaevskii equation is taken to be the one-dimensional one from Eq. (3.18), where $a_\perp$ is the transverse width of the Bose-Einstein Condensate. In the following, the number of (Rubidium-)atoms is $10^2$ and $a_\perp = 10\,\mu m$. This leads to a scaled interaction term $g = 0.15$. The other parameters are the same as in Sec. 4.2: $\hbar = 1.2649$, $F = 0.0036$. For this case Fig. 4.18 shows the average position over time. A damping due to the mean-field term is clearly visible.

As shown in Sec. 4.2, a disordered potential realized with a bichromatic optical lattice also damps the Bloch oscillations. There is however an interesting interplay between disorder and interaction. To explore this interplay

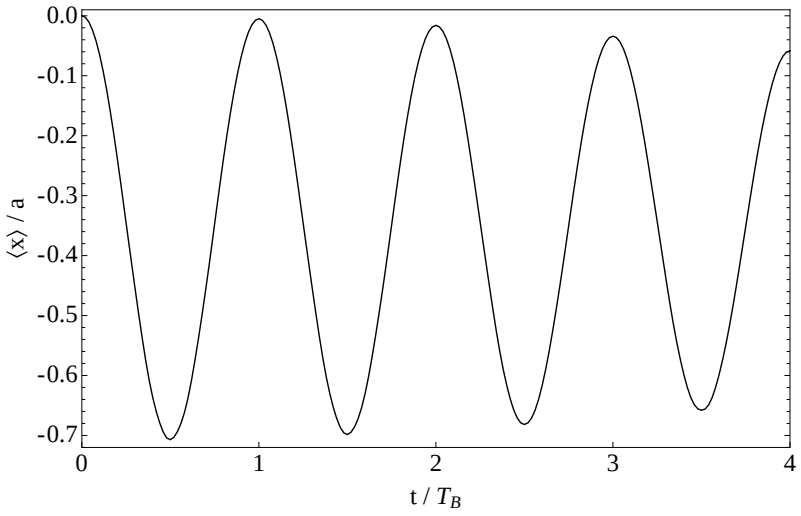


Figure 4.18: **Damped Bloch oscillations in a system with interactions.** The nonlinear term in Eq. (4.30) is a measure for the interaction between atoms in a Bose-Einstein Condensate and leads to a damping of the Bloch oscillations.

we fix the parameters which describe the disorder in the bichromatic lattice to $s = 0.0005$ and $\alpha = 0.4$, and vary the interaction term $g$. Fig. 4.19 summarizes the results of a numerical simulation of the system

$$i\,\hbar\,\partial_t\,\psi(x,t) = \left(-\frac{\hbar^2}{2}\frac{d^2}{dx^2} + \cos(x) + s\cos(\alpha x) + Fx + g\,|\psi(x,t)|^2\right)\,\psi(x,t)\,. \tag{4.31}$$

It can be seen that due to an increase of the interaction term, the damping of the Bloch oscillations decreases. If however the interaction is getting too strong, the damping of the Bloch oscillations is governed by the interaction term. This also has been investigated in [31, 32], where the disorder was realized with speckle patterns.

To gain more insight into why Bloch oscillations are damped due to disorder or interaction, and why they can cancel each other out, we expand upon a simple model which was introduced in [33]. This model is a tight binding one and describes the influence of the nonlinear term in the Gross-Pitaevskii equation on the Bloch oscillations fairly well. In this tight binding approximation the wave function $\psi(x,t)$ in the Gross-Pitaevskii equation Eq. (3.17)

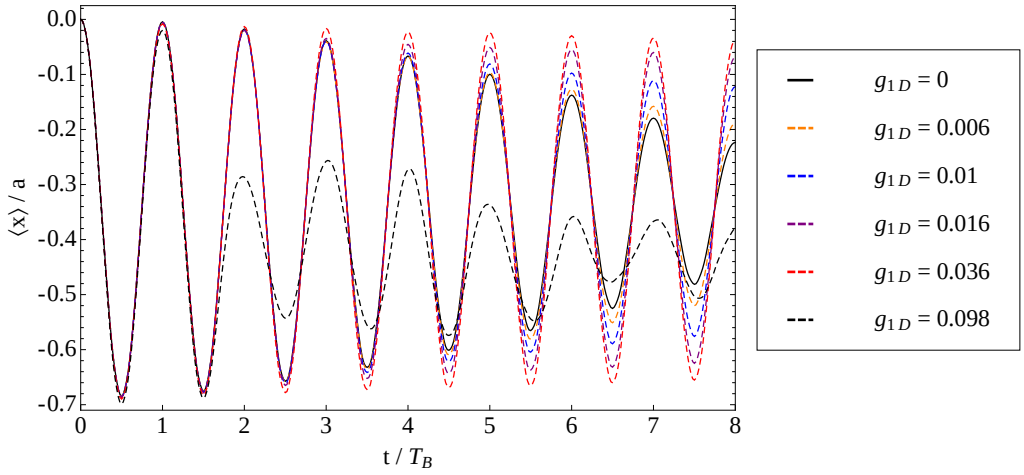


Figure 4.19: **Interplay between disorder and interaction.** An increasing nonlinearity counteracts the disorder and leads to less damped Bloch oscillations, up to a point where the damping of the Bloch oscillations is then dominated by the nonlinearity.

is expanded in Wannier functions $w(x - x_n)$ from only the lowest Bloch band

$$\psi(x,t) = \sum_n \Psi_n(t) w(x - x_n)\,, \tag{4.32}$$

where $\Psi_n(t)$ is a time dependent amplitude and the Wannier functions $w(x - x_n)$ are localized wave functions in each well $n$. The potential $V(x)$ in Eq. (3.17) has now the form $V(x) = V_{periodic}(x) + V_{ext}(x)$. We are using the ansatz Eq. (4.32) in the Gross-Pitaevskii equation Eq. (3.17) and the result is the discrete nonlinear Schrödinger equation

$$i\hbar\partial_t \Psi_n = -J\left(\Psi_{n-1} + \Psi_{n+1}\right) + V_n \Psi_n + g|\Psi_n|^2 \Psi_n\,, \tag{4.33}$$

where $J$ is the tunneling probability for neighboring sites (in the tight binding approximation $J = \Delta/4$, with $\Delta$ being the bandwidth of the lowest Bloch band) and $V_n$ describing the external potential. The model in [33] uses a classical Hamiltonian approach to describe the time dependent Schrödinger equation Eq. (4.33). Therefore, we can identify Eq. (4.33) as an equation of motion to

$$\dot{\Psi}_n = \frac{\partial H'}{\partial i\hbar \Psi_n^*}\,, \tag{4.34}$$

with the conjugate variables $i\hbar\Psi_n^*$ and $\Psi_n$ and the Hamiltonian

$$H' = \sum_n \left[ -J\left(\Psi_n \Psi_{n+1}^* + \Psi_n^* \Psi_{n+1}\right) + V_n |\Psi_n|^2 + \frac{g}{2}|\Psi_n|^4 \right] . \tag{4.35}$$

As also proposed in [33], we study the dynamical behavior of Eq. (4.35) with a semiclassical variational approach. The variational wave function is a Gaussian profile wave packet

$$\Psi_{n,var}(t) = \left(\frac{2}{\gamma^2\pi}\right)^{\frac{1}{4}} e^{ip(n-\xi) - \frac{(n-\xi)^2}{\gamma^2} + i\frac{\delta^2}{2}(n-\xi)^2} , \tag{4.36}$$

with variational parameters $\xi(t)$ and $p(t)$ being the center and its momentum of the wave packet and $\gamma(t)$ and $\delta(t)$ being the width and its momentum of the wave packet. The equations of motions to the variational parameters are given by

$$\frac{d}{dt}\frac{\partial L}{\partial \dot{q}_i} = \frac{\partial L}{\partial q_i} , \tag{4.37}$$

with the Lagrangian

$$L = \sum_n i\hbar \dot{\Psi}_n \Psi_n^* - H' . \tag{4.38}$$

The equations of motion for the $q_i(t) = \xi(t), p(t), \gamma(t), \delta(t)$ are then derived as

$$\dot{p} = -\frac{1}{\hbar}\frac{\partial V(\gamma,\xi)}{\partial \xi} \tag{4.39}$$

$$\dot{\xi} = 2J\frac{1}{\hbar}\sin(p)e^{-\eta} \tag{4.40}$$

$$\dot{\gamma} = 2J\frac{1}{\hbar}\gamma\delta\cos(p)e^{-\eta} \tag{4.41}$$

$$\dot{\delta} = 2J\frac{1}{\hbar}\left(\frac{4}{\gamma^4} - \delta^2\right)\cos(p)e^{-\eta} + \frac{2g}{\sqrt{\pi}\gamma^3} - \frac{4}{\gamma}\frac{\partial V(\gamma,\xi)}{\partial \gamma} , \tag{4.42}$$

with

$$\eta = \frac{1}{2\gamma} + \frac{\gamma^2\delta^2}{8} , \tag{4.43}$$

and $V(\gamma,\xi)$ describing the external potential $V_n$

$$V(\gamma,\xi) = \left(\frac{2}{\gamma^2\pi}\right)^{\frac{1}{2}} \int_{-\infty}^{\infty} dn\, V_n e^{-\frac{2(n-\xi)^2}{\gamma^2}} . \tag{4.44}$$

The effective Hamiltonian for the conjugate variables $\xi$, $p$ and $\gamma/8, \delta$ reads

$$H = -J\cos(p)e^{-\eta} + V(\gamma,\xi) + \frac{g}{2\sqrt{\pi}\gamma}\,. \tag{4.45}$$

We are also able to define a group velocity of the wave packet

$$v_g = \partial H/\partial p = \dot{\xi} = \tan(p)/m^* \tag{4.46}$$

and with that, an effective inverse mass

$$(m^*)^{-1} = \partial^2 H/\partial p^2 = \cos(p)e^{-\eta}\,. \tag{4.47}$$

The external potential $V_n$ in the case of a tilted disordered potential generated by a bichromatic optical lattice has the form

$$V_n = Fn - s\cos(\alpha n)\,. \tag{4.48}$$

With this we can easily integrate Eq. (4.44) and the resulting $V(\gamma,\xi)$ can be plugged into the equations of motion Eq. (4.39) and Eq. (4.42). It should be mentioned that the potential Eq. (4.48) differs from the one used in Eq. (4.31) by the minus sign in front of the term $s\cos(\alpha x)$. The exact numerical simulation of Eq. (4.31) shows that this sign does not affect the result, but it is necessary in this section to describe the correct interplay between disorder and interaction. We can see in Eq. 4.51 or Eq. 4.53 that we need the minus sign, so that the interaction can cancel the damping effect due to disorder. This model is only thought of as an illustrative one. It does not reproduce the independence on the sign of $s$, as it is observed in the exact numerical simulation of the system. With this, the resulting coupled equations can then be solved numerically for each of the variational parameters.

More insight in the dynamics is gained by looking at the second order differential equation for $\xi(t)$. We therefore take the time derivative of Eq. (4.40) and plug in the expressions for $\dot{\gamma}$ and $\dot{\xi}$, which leads us to

$$\ddot{\xi} + \left(\frac{g\delta}{2\hbar\sqrt{\pi}\gamma} - \frac{1}{4\hbar}\alpha^2 s\delta\gamma^2\cos(\alpha\xi)e^{-\frac{1}{8}\alpha^2\gamma^2}\right)\dot{\xi} + \tag{4.49}$$

$$+\frac{2J}{\hbar^2}e^{-\eta}\cos(p)\left(F + \alpha s\sin(\alpha\xi)e^{-\frac{1}{8}\alpha^2\gamma^2}\right) = 0\,. \tag{4.50}$$

This reminds one of the differential equation of a damped oscillator, where we

can define a damping term $\beta$

$$\beta = \frac{g\delta}{2\hbar\sqrt{\pi}\gamma} - \frac{1}{4\hbar}\alpha^2 s\delta\gamma^2 \cos(\alpha\xi)e^{-\frac{1}{8}\alpha^2\gamma^2} \,. \tag{4.51}$$

To understand why the Bloch oscillations are damped out, the limits of $\gamma(t)$ and $\delta(t)$ for $t \to \infty$ are necessary. From the numerical solution of the equations of motions Eq. (4.39) to Eq. (4.42) we see that the width of the wave packet tends to a constant value $\gamma_\infty$, not very different from $\gamma(t=0)$. The center of the wave packet also tends to a constant value $\xi_\infty$, which is equal to the amplitude of the undamped Bloch oscillations. With this, $\delta$ has a time dependance that goes as

$$\delta \sim \left(\frac{1}{\hbar}\frac{2g}{\sqrt{\pi}\gamma_\infty^3} - \alpha^2 s\cos(\alpha\xi_\infty)e^{-\frac{1}{8}\alpha^2\cdot\gamma_\infty^2}\right) t \,. \tag{4.52}$$

The effective mass $m^*$ is also a time dependent variable and for the limit $t \to \infty$ it goes as

$$m^* \sim e^{\frac{\gamma_\infty^2}{8\hbar^2}t^2\left(\frac{2g}{\sqrt{\pi}\gamma_\infty^3} - \alpha^2 s\cos(\alpha\xi_\infty)e^{-\frac{1}{8}\alpha^2\gamma_\infty^2}\right)^2} \,. \tag{4.53}$$

With this background the damping of the Bloch oscillations could be thought of a diverging effective mass $m^*$. In Eq. (4.53) one can also see that disorder and interaction can cancel each other out if the exponential becomes zero, or equal the damping term $\beta = 0$, which is the case if

$$g = \frac{1}{2}\sqrt{\pi}\gamma_\infty^3\alpha^2 s\cos(\alpha\xi_\infty)e^{-\frac{1}{8}\alpha^2\gamma_\infty^2} \,. \tag{4.54}$$

Within this approximation and the approximations made in the limit for $t \to \infty$, we find that Eq. (4.54) describes the cancellation of disorder and interaction remarkably well. This model is however not in exact agreement with the results of the exact numerical calculation. We use it as an illustrative method to explain the possibility of the counteracting effect of interaction on disorder. We are also able to understand the dependance on $e^{-t^2}$ of the fit function Eq. (4.5), using this model, see Eq. (4.53).

To conclude this section, we were able to show with exact numerical calculations, that interactions can counteract the damping of Bloch oscillations caused by disorder. A variational principle of the discrete nonlinear Schrödinger equation Eq. (4.33) lead to the equations of motion of the variational parameters which can be solved numerically. With Eq. (4.54), an expression was found to predict the value of the interaction necessary to neutralize the damping of

Bloch oscillations due to disorder described by the parameters $\alpha$ and $s$.

# Chapter 5

# Conclusion

We have investigated the influence of disorder in an optical lattice on Bloch oscillations. To gain information on the dynamics of the system we had to solve the time dependent Schrödinger equation, which was done by the Split Operator Method.

It could be shown that the damping of Bloch oscillations is dependent on the form of disorder present in the system.

In the case of the bichromatic optical lattice the Bloch oscillations were damped nicely and showed a revival. We also investigated the dependance of the damping on the parameters $\alpha$ and $s$, which describe the disorder. The expected increase in the damping of the Bloch oscillations for an increasing strength of the disorder $s$ is clearly observable in the numerical simulations. Changing the parameter $\alpha$ has a non-trivial influence on the damping of Bloch oscillations. For certain special values of $\alpha$, no damping is expected, which we have observed and explained.

For a realization of disorder by impurities on distinct lattices sites, it was shown that a periodic pattern of impurities leads to a new unit cell in the lattice and to a new Bloch time $T_B$. A slightly distorted periodic pattern damps the Bloch oscillations, but not drastically. We were also able to show that a totally random distribution of impurities in the lattice is heavily affecting the Bloch oscillations. If the concentration of impurities is large enough, the Bloch oscillations will be destroyed completely.

Future work on the topic should contain a more analytical approach, to quantify the damping in terms of the disorder parameter. This is also important when it comes to the interplay between disorder and interactions.

# Bibliography


[1] F. Bloch. Über die Quantenmechanik der Elektronen in Kristallgittern. *Z. Phys.*, 52:555, 1928.

[2] J. Feldmann, K. Leo, J. Shah, D. A. B. Miller, J. E. Cunningham, T. Meier, G. von Plessen, A. Schulze, P. Thomas, and S. Schmitt-Rink. Optical investigation of Bloch oscillations in a semiconductor superlattice. *Phys. Rev. B*, 46:7252, 1992.

[3] C. Waschke, H.G. Roskos, R. Schwedler, K. Leo, H. Kurz, and K. Köhler. Coherent submillimeter-wave emission from Bloch oscillations in a semiconductor superlattice. *Phys. Rev. Lett.*, 70:3319, 1993.

[4] V. G. Lyssenko, G. Valusis, F. Löser, T. Hasche, K. Leo, M.M Dignam, and K. Köhler. Direct Measurement of the Spatial Displacement of Bloch-Oscillating Electrons in Semiconductor Superlattices. *Phys. Rev. Lett.*, 79: 301, 1997.

[5] B. P. Anderson and M. A. Kasevich. Macroscopic Quantum Interference from Atomic Tunnel Arrays. *Science*, 27:1686, 1998.

[6] M. Cristiani, O. Morsch, J. H. Müller, D. Ciampini, and E. Arimondo. Experimental properties of Bose-Einstein condensates in one-dimensional optical lattices: Bloch oscillations, Landau-Zener tunneling, and mean-field effects. *Phys. Rev. A*, 65:063612, 2002.

[7] O. Morsch, J.H. Müller, M. Cristiani, D. Ciampini, and E. Arimondo. Bloch Oscillations and Mean-Field Effects of Bose-Einstein Condensates in 1D Optical Lattices. *Phys. Rev. Lett.*, 87:140402, 2001.

[8] M. Ben Dahan, E. Peik, J. Reichel, Y. Castin, and C. Salomon. Bloch Oscillations of Atoms in an Optical Potential. *Phys. Rev. Lett.*, 76:4508, 1996.

[9] C. F. Bharucha, K. W. Madison, P. R. Morrow, S. R. Wilkinson, B. Sundaram, and M. G. Raizen. Observation of atomic tunneling from an accelerating optical potential. *Phys. Rev. A*, 55:R857, 1997.

[10] K.W. Madison, M.C. Fischer, and M.G. Raizen. Observation of the Wannier-Stark fan and the fractional ladder in an accelerating optical lattice. *Phys. Rev. A*, 60:R1767, 1999.

[11] E. Peik, M. Ben Dahan, I. Bouchoule, Y. Castin, and C. Salomon. Bloch oscillations of atoms, adiabatic rapid passage, and monokinetic atomic beams. *Phys. Rev. A*, 55:2989, 1997.

[12] S.R. Wilkinson, C. F. Bharucha, K. W. Madison, Q. Niu, and M. G. Raizen. Observation of Atomic Wannier-Stark Ladders in an Accelerating Optical Potential. *Phys. Rev. Lett.*, 76:4512, 1996.

[13] Q. Niu, X. Zhao, G. A. Georgakis, and M. G. Raizen. Atomic Landau-Zener Tunneling and Wannier-Stark Ladders in Optical Potentials. *Phys. Rev. Lett.*, 76:4504, 1996.

[14] V. V. Konotop, P. G. Kevrekidis, and M. Salerno. Landau-Zener tunneling of Bose-Einstein condensates in an optical lattice. *Phys. Rev. A*, 72: 023611, 2005.

[15] N. David Mermin Neil W. Ashcroft. *Solid State Physics*. Saunders College Publishing, 1976.

[16] C. Zener. A Theory of the Electrical Breakdown of Solid Dielectrics. *Proc. R. Soc. Lond. A*, 145:523, 1934.

[17] G. H. Wannier. Wave Functions and Effective Hamiltonian for Bloch Electrons in an Electric Field. *Phys. Rev.*, 117:432, 1960.

[18] J. B. Krieger and G. J. Iafrate. Time evolution of Bloch electrons in a homogeneous electric field. *Phys. Rev. B*, 33:5494, 1986.

[19] A. M. Bouchard and M. Luban. Bloch oscillations and other dynamical phenomena of electrons in semiconductor superlattices. *Phys. Rev. B*, 52: 5105, 1995.

[20] Gerard J. Milburn D. F. Walls. *Quantum Optics*. Springer, 2008.

[21] N. Bogoliubov. Theory of superfluidity. *J. Phys. USSR*, 11:23, 1947.

[22] O. Morsch and M. Oberthaler. Dynamics of Bose-Einstein condensates in optical lattices. *Rev. Mod. Phys.*, 78:179, 2006.

[23] P. Meystre. *Atom Optics*. Springer, 2001.

[24] J. E. Lye, L. Fallani, M. Modugno, D. S. Wiersma, C. Fort, and M. Inguscio. Bose-Einstein Condensate in a Random Potential. *Phys. Rev. Lett.*, 95:070401, 2005.

[25] L. Fallani, J. E. Lye, V. Guarrera, C. Fort, and M. Inguscio. Ultracold Atoms in a Disordered Crystal of Light: Towards a Bose Glass. *Phys. Rev. Lett.*, 98:130404, 2007.

[26] U. Gavish and Y. Castin. Matter-Wave Localization in Disordered Cold Atom Lattices. *Phys. Rev. Lett.*, 95:020401, 2005.

[27] M. D. Feit, J. A. Fleck Jr., and A. Steiger. Solution of the Schrödinger equation by a spectral method. *Journal of Computational Physics*, 47: 412, 1982.

[28] M. Holthaus. Bloch oscillations and Zener breakdown in an optical lattice. *Journal of Optics B: Quantum and Semiclassical Optics*, 2:589, 2000.

[29] D. Witthaut, M. Werder, S. Mossmann, and H.J. Korsch. Bloch oscillations of Bose-Einstein condensates: Breakdown and revival. *Phys. Rev. E*, 71:036625, 2005.

[30] P. W. Anderson. Absence of Diffusion in Certain Random Lattices. *Phys. Rev.*, 109:1492, 1958.

[31] S. Drenkelforth, G. Kleine Buning, J. Will, T. Schulte, N. Murray, W. Ertmer, L. Santos, and J. J. Arlt. Damped Bloch oscillations of Bose-Einstein condensates in disordered potential gradients. *New Journal of Physics*, 10:045027, 2008.

[32] T. Schulte, S. Drenkelforth, G. Kleine Buning, W. Ertmer, J. Arlt, M. Lewenstein, and L. Santos. Dynamics of Bloch oscillations in disordered lattice potentials. *Physical Review A*, 77:023610, 2008.

[33] A. Trombettoni and A. Smerzi. Discrete Solitons and Breathers with Dilute Bose-Einstein Condensates. *Phys. Rev. Lett.*, 86:2353, 2001.

[34] R. H. Bisseling, R. Kosloff, and J. Manz. Dynamics of hyperspherical and local mode resonance decay studied by time dependent wave packet propagation. *The Journal of Chemical Physics*, 83:993, 1985.

[35] D. Neuhasuer and M. Baer. The time-dependent Schrödinger equation: Application of absorbing boundary conditions. *The Journal of Chemical Physics*, 90:4351, 1989.

# Appendix A

# Units

## A.1 Units used for numerical calculations

In the following, we are giving a description of the used scaled units. The system of units is motivated by the used cosine-potential and by reducing the number of free parameters to a minimum. Considered is the Gross-Pitaevskii equation which describes the wave function of a Bose-Einstein Condensate

$$i\hbar\partial_t\psi(x,t) = \left[-\frac{\hbar^2}{2m}\frac{\partial^2}{\partial x^2} + V(x) + Fx + g\,|\psi(x,t)|^2\right]\psi(x,t)\,. \tag{A.1}$$

The scaled mass is taken to be $m_s = 1$ and the period of the potential is chosen as $a_s = 2\,\pi$. The energy scale is set that the potential varies in the interval $[-1, 1]$. With these conditions we can simply write the potential in scaled units as $V_s(x_s) = \cos(x_s)$. With the scaled space coordinate $x_s = (2\pi/a)\,x$, the period of $V_s$ is $2\pi$. We are now defining $\bar{V} = V_0/2$. Dividing Eq. (A.1) by $\bar{V}$ and replacing $x$ by $x_s$ we arrive at at the scaled Gross-Pitaevskii equation

$$i\hbar_s\partial_{t_s}\psi(x_s,t_s) = \left[-\frac{\hbar_s^2}{2}\frac{\partial^2}{\partial x_s^2} + V_s(x_s) + F_s x_s + g_s\,|\psi(x_s,t_s)|^2\right]\psi(x_s,t_s)\,, \tag{A.2}$$

with the following conversion rules

$$\hbar_s = \frac{2\pi}{a\sqrt{m\bar{V}}}\,\hbar \tag{A.3}$$

$$F_s = \frac{a}{2\pi\bar{V}}\,F \tag{A.4}$$

$$g_s = \frac{2\pi}{\bar{V}a}\,g \tag{A.5}$$

$$t_s = \frac{2\pi}{a}\sqrt{\frac{\bar{V}}{m}}\,t\,. \tag{A.6}$$

The Bloch period $T_B$ becomes

$$T_B = \frac{2\pi\hbar}{aF} \tag{A.7}$$

$$T_{B,s} = \frac{\hbar_s}{F_s}\,. \tag{A.8}$$

The actual period of the optical lattice is $a = \lambda_L/2$ where $\lambda_L$ is the wavelength of the laser generating the optical lattice. Given the recoil energy $E_r = \hbar^2 k_L^2/2m$, here $k_L$ is the wave number of the laser and knowing the depth of the optical lattice $V_0$ in recoil energies, we can evaluate the scaled Planck constant to

$$\hbar_s = \frac{4}{\sqrt{V_0/E_r}}\,. \tag{A.9}$$

The parameters in this thesis are chosen in order to resemble the experimental values in the group of Dominik Schneble here at Stony Brook. Tab. A.1 summarizes the used values. The strength of the force $Fg$ was chosen $0.2\,Fg$ in oder to ensure that Zener-tunneling is negligible.

| $\lambda_L/nm$ | $V_0/E_R$ | $0.2\,Fg/E_R$ | $\hbar_s$ | $F_s$ |
|---|---|---|---|---|
| 1064 | 10 | 0.5604 | 1.2649 | 0.0036 |

Table A.1: **Summary of used parameters.** The parameters are chosen to represent the experimental ones in Dominik Schneble's group at Stony Brook.

# Appendix B

# Numerical methods

## B.1 Solving the stationary Schrödinger equation for Bloch bands and Bloch functions

In this section a description is given how the Schrödinger equation Eq. (2.1) with a periodic potential $V(x+a) = V(x)$ can be solved numerically. The periodic potential throughout this thesis is a cosine-potential $V(x) = \cos(x)$. The Hamiltonian on the left hand side of Eq. (2.1) can easily be solved in a plane wave basis. The matrix elements then read

$$H_{i,j} = \frac{\hbar^2}{2}\left(k - \frac{2\pi}{a}j\right)^2 \delta_{i,j} + \frac{V_0}{2}\left(\delta_{i,j+1} + \delta_{i,j-1}\right) . \tag{B.1}$$

The obtained matrix can then be diagonalized for each allowed $k$-value leading to the eigenvalues $E_n(k)$, where $n$ denotes the band index. An implementation in *Mathematica* is shown in the following lines. Tab. B.1 summarizes the arguments appearing in the functions.

The function `kVEC[...]` defines the allowed $k$-values:

```
kVEC[counterk_, a_, lengthsys_] :=
  Module[{countk, A, NN},
  countk = counterk;
  A = a;
  NN = lengthsys;

  kv = N[2*Pi*countk/NN/A];
  Return[kv];
]
```

The next function `KLattice[...]` defines the reciprocal lattice vector:

| Parameter | Meaning |
|---|---|
| `counterk` | counter variable for $k$ |
| `counterK` | counter variable for $K$ |
| `a` | lattice constant |
| `lengthsys` | length to discretize $k$-values |
| `hbar` | scaled Plack's constant |
| `U0` | depth of lattice, with scaled units always one |
| `kk` | distinct $k$-value |
| `size` | determines the size $(2\,size + 1)$ of the matrix |
| `sigma` | width of wave function to be projected onto a Bloch band |

Table B.1: **Summary of arguments.** The number of parameters is intended to be kept small.

```
KLattice[counterK_, a_] := Module[{countK, A},
  countK = counterK;
  A = a;

  KL = N[2*Pi*countK/A];
  Return[KL];
]
```

The matrix (2.17) is generated using the function `SetMatrix[...]\verb`:

```
SetMatrix[hbar_, U0_, a_, kk_, size_] :=
 Module[{h, ampCos, ampCos2, A, s, ki, matrixSize},
  h = hbar;
  ampCos = U0;
  A = a;
  ki = kk;
  matrixSize = size;

  matrix =
   Table[0.5*h^2*(ki - KLattice[i, A])*(ki - KLattice[i, A])*
      KroneckerDelta[i, j] +
     0.5*ampCos*(KroneckerDelta[(i - j) - 1] +
        KroneckerDelta[(i - j) + 1]), {i, -matrixSize,
     matrixSize}, {j, -matrixSize, matrixSize}];
  Return[N[matrix]];
]
```

The last function `bands[...]` diagonalizes the matrices Eq. (2.17) for every $k$-value. With evaluating the function `bands[...]`, the calculated Bloch bands are stored in `band[n]` and Bloch functions can be plotted using the function `blochFunction[kindex, bandindex, x]`.

```
bands[hbar_, U0_, a_, lengthsys_, size_] :=
 Module[{h, ampCos, A, NN, matrixSize},
  h = hbar;
  ampCos = U0;
  A = a;
  matrixSize = size;
  NN = lengthsys;

  delk = 1/NN;

  kTable = Table[kVEC[m, A, NN], {m, -NN/2 + 1, NN/2}];

  eigenSYS =
   Thread[{Table[kVEC[m, A, NN], {m, -NN/2 + 1, NN/2}],
     Table[Sort[
       Transpose[
        Eigensystem[
         SetMatrix[h, ampCos, A, kVEC[m, A, NN], matrixSize]]],
       Re[#1[[1]]] < Re[#2[[1]]] &], {m, -NN/2 + 1, NN/2}]}];

  blochFunction[kindex_, bandindex_, x_] :=
   Exp[I*eigenSYS[[kindex, 1]]*x]*
    Sum[eigenSYS[[All, 2, bandindex]][[kindex, 2,
      sumindex]], {sumindex, 1, (2*matrixSize + 1)}];

  For[o = 1, o <= (2*matrixSize + 1), o++,
   band[o] =
     Transpose[
      Join[{eigenSYS[[All, 1]]}, {eigenSYS[[All, 2, o]][[All, 1]]}]];
   ];

  plotList = Table[band[t], {t, 1, (2*matrixSize + 1)}];

]
```

We are now discussing the projection of any initial wave function $|\Psi_0\rangle$ onto a distinct Bloch band $n$. The following ansatz is made, with $|\Psi_n\rangle$ being the projected wave function

$$|\Psi_n\rangle = \int_{BZ} dk \, \langle \phi_{n,k}| \, |\Psi_0\rangle \, |\phi_{n,k}\rangle \,, \tag{B.2}$$

where

$$|\phi_{n,k}\rangle = \sum_i c_{n,i}(k) \; |K_i + k\rangle \,, \tag{B.3}$$

is the Fourier expansion of the Bloch function in plane waves. The $c_{n,i}(k)$ are the entries (labeled $i$) of the eigenvectors to the corresponding $k$-value of band

$n$, resulting from the diagonalization of the matrix Eq. (2.17). We can write the scalar product in Eq. (B.2) as

$$\langle \phi_{n,k} | \, | \Psi_0 \rangle = \beta_n(k) = \sum_i c^*_{n,i}(k) \, \langle K_i + k | \, | \Psi_0 \rangle \tag{B.4}$$

$$= \sum_i c^*_{n,i}(k) \tilde{\Psi}(K_i + k) \, , \tag{B.5}$$

with $\tilde{\Psi}(K_i + k)$ being the representation of $\Psi_0$ in momentum space. The projection in the end reads

$$\tilde{\Psi}_n(k') = \int_{BZ} dk \, \beta_n(k) \, c_{n,i}(k) \, , \tag{B.6}$$

$k' = (K_i + k)$. The code in *Mathematica* is shown below. It uses a normalized Gaussian of the form Eq. (4.2) as $|\Psi_0\rangle$. The only input to the function `blochPRO[...]` is the width $\sigma$ of the Gaussian. In the code below the wave function is projected onto the ground band.

```
blochPRO[sigma_] := Module[{widthPsi},
      widthPsi = sigma;

      (* coeff of matrix diagonalization *)
  blochcoeff1 =
   Flatten[Table[
     Reverse[eigenSYS[[All, 2, 1, 2, i]]], {i, 1,
      Length[eigenSYS[[1, 2, 1, 2]]]}]];

      (* psi init in momentum space *)
  psi0 = N[(2/Pi)^0.25*widthPsi^0.5*Exp[-widthPsi^2*kGrid^2]];

      (* cut blochcoeff to have same length as psi0 *)
  cut = (Length[blochcoeff1] - Length[psi0])/2;

  blochcoeffcut1 =
   blochcoeff1[[cut + 1 ;; Length[blochcoeff1] - cut]];

      (* init psipro and coeff for psipro*)
  psiPROk1 = Table[0, {Length[psi0]}];
  b1 = Table[0, {Length[kTable]}];
  indexmax = Floor[(Length[psi0]/Length[kTable] - 1)/2];
  index =
   Table[i, {i, -indexmax, indexmax}]*
     Length[kTable] + (Length[psi0] - Length[kTable])/2;

      For[counter = 1, counter <= Length[kTable], counter++,
         b1[[counter]] =
```

```
    blochcoeffcut1[[index + counter]].psi0[[index + counter]];
         psiPROk1[[index + counter]] =
    b1[[counter]]*blochcoeffcut1[[index + counter]];
         ];

  psiPROkend = psiPROk1;

      (* transform psiPROk to real space *)
  psiPROkendrot = RotateLeft[psiPROkend, Length[psiPROkend]/2 - 1];
      psiPROxend =
   Chop[RotateRight[Fourier[psiPROkendrot], Length[psiPROkend]/2 - 1]];
]
```

## B.2 The Split Operator Method

The Split-Operator Method [27] is a technique for propagating a wave function in time, *i. e.* to solve the time dependent Schrödinger equation

$$i\hbar\,\partial_t\,\Psi(t) = \hat{H}\,\Psi(t) = (\hat{T} + \hat{V})\,\Psi(t)\,. \tag{B.7}$$

The main idea behind this technique is that the action of the quantum mechanical position-operator is a multiplication in coordinate space and the action of the quantum mechanical momentum operator is a multiplication in momentum space. Switching between coordinate space and momentum space is done by a Fast Fourier transform. Given an explicitly time independent Hamiltonian as in Eq. (B.7) the formal solution to the time dependent Schrödinger equation is given by

$$\Psi(t) = \hat{U}(t, t_0)\,\Psi(t_0) \tag{B.8}$$

where U is the time-evolution operator

$$\hat{U}(t, t_0) = e^{-\frac{i}{\hbar}\hat{H}(t-t_0)}. \tag{B.9}$$

For one time step $\Delta t$ of the evolution, Eq. (B.8) becomes with Eq. (B.9)

$$\Psi(t + \Delta t) = e^{-\frac{i}{\hbar}(\hat{T}+\hat{V})\Delta t}\,\Psi(t)\,. \tag{B.10}$$

We cannot write the exponential of the sums in Eq. (B.10) as a product of exponentials because the kinetic energy operator $\hat{T} \sim \hat{p}$ does not commute with the potential energy operator $\hat{V} \sim \hat{x}$.

But in oder to apply the above mentioned fast Fourier transform the exponential in (B.10) has to be split. We are doing this by applying the Baker-Campbell-Hausdorff formula and in order to keep the error small, the Baker-

Campbell-Hausdorff formula for three operators is considered

$$e^{\hat{A}}e^{\hat{B}}e^{\hat{C}} = e^{\hat{A}+\hat{B}+\hat{C}+\frac{1}{2}[\hat{A};\hat{B}]+\frac{1}{2}[\hat{A};\hat{C}]+\frac{1}{2}[\hat{B};\hat{C}]+\frac{1}{12}[[\hat{A};\hat{B}];\hat{A}+\hat{B}+\hat{C}]+\ldots}\,. \tag{B.11}$$

We are applying Eq. (B.11) to the exponential in (B.10) and arrive at

$$\begin{aligned} e^{-\frac{i}{\hbar}\hat{H}\Delta t} &= e^{\tilde{T}+\tilde{V}} = e^{\tilde{T}/2+\tilde{V}+\tilde{T}/2} && \text{(B.12)}\\ &= e^{\tilde{T}/2}e^{\tilde{V}+\tilde{T}/2}e^{-1/2[\tilde{T}/2;\tilde{T}/2+\tilde{V}]+O(\Delta t^3)} && \text{(B.13)}\\ &= e^{\tilde{T}/2}e^{\tilde{V}+\tilde{T}/2}e^{-1/2[\tilde{T}/2;\tilde{V}]+O(\Delta t^3)} && \text{(B.14)}\\ &= e^{\tilde{T}/2}e^{\tilde{V}}e^{\tilde{T}/2}e^{-1/2[\tilde{V};\tilde{T}/2]+O(\Delta t^3)}e^{-1/2[\tilde{T}/2;\tilde{V}]+O(\Delta t^3)} && \text{(B.15)}\\ &= e^{\tilde{T}/2}e^{\tilde{V}}e^{\tilde{T}/2}e^{O(\Delta t^3)}\,, && \text{(B.16)} \end{aligned}$$

where we have substituted $\tilde{H} = -\frac{i}{\hbar}\hat{H}\Delta t$. The evolution over one time step of the wave function now becomes

$$\Psi(t+\Delta t) = e^{-\frac{i}{\hbar}\hat{T}/2\Delta t}e^{-\frac{i}{\hbar}\hat{V}\Delta t}e^{-\frac{i}{\hbar}\hat{T}/2\Delta t}\,\Psi(t)\,, \tag{B.17}$$

with an error $\sim \Delta t^3$. To keep the error of order $\Delta t^3$, we split the kinetic energy part of the Hamiltonian in half. We could also have done this with the potential energy operator, which was actually done in the code below. An implementation of this technique in *Mathematica* is shown in the following lines.

```
(* time evolution operator part for potential on x-grid *)
Vop[delt] = N[Exp[-0.5*I*delt*modelV/hbar]];

(* time evolution operator part for kinetic energy on k-grid *)
Kop[delt] = N[Exp[-0.5*I*delt*hbar*kGridROT*kGridROT]];

(* here psi is the wave packet on the x-Grid at time t *)
U[delt_]@psi_ :=
  Chop[Vop[delt]*
    RotateRight[
     Fourier[Kop[
        delt]*(Chop[
         InverseFourier[RotateLeft[Vop[delt]*psi, n/2 - 1]]])],
     n/2 - 1]];

(* propagation of psi forward in time over nt steps by applying U[delt] *)
psi[nt_, psi0_] := Nest[U[delt][#] &, psi0, nt];
Do[psi[nt] = psi[tout, psi[nt - tout]], {nt, tout, stepsmax, tout}];
```

During the time evolution of an initial wave packet, it could be possible that the wave packet reaches the grid edge and gets reflected back into the system.

This unphysical behavior can be prevented by multiplying the propagated wave function each time step with a function that is equal to one over the part of the grid where the evolution takes places and is smoothly going to zero at the grid boundaries [34]. Another possibility is placing an absorbing potential at the grid boundaries [35]. This potential has to be negative and imaginary. The second approach is much faster than the first one because the absorbing potential has to be add only once before the propagation. We use the potential proposed in [35]

$$V_{abs} = \begin{cases} -i\, V_{abs,0}\, \frac{x-x_0}{\delta x} & \text{for } x_0 < x \leq x_0 + \delta x \\ 0 & \text{for } x \leq x_0\,. \end{cases} \tag{B.18}$$

$V_{abs,0}$ is the amplitude of the potential $V_{abs}$. $x_0$ is the beginning of the potential and $\delta x$ is the width of the absorbing potential. $V_{abs,0}$ and $\delta x$ can approximately be determined by an estimation made in [35], but for perfect absorption one has to try different values for the parameters.

## B.3 The Split Operator Technique for the nonlinear Schrödinger equation

The Gross-Pitaevskii equation is a nonlinear Schrödinger equation where we can interpret the nonlinear term $g\,|\Psi(x,t)|^2 = V_g(x,t)$ as a second time dependent potential

$$i\,\hbar\,\partial_t\,\Psi(x,t) = \left(\hat{T} + \hat{V} + g\,|\Psi(x,t)|^2\right)\,\Psi(x,t) \tag{B.19}$$

$$= \left(\hat{T} + \hat{V} + \hat{V}_g(x,t)\right)\,\Psi(x,t) \tag{B.20}$$

$$= \hat{H}(t)\,\Psi(x,t)\,. \tag{B.21}$$

The time evolution operator for an evolution $t = t' = 0 \rightarrow t = t'' = \Delta t$ is given by

$$\Psi(\Delta t) = \hat{U}(\Delta t)\,\Psi(0)\,, \tag{B.22}$$

and also fulfills a time dependent Schrödinger equation

$$i\hbar\,\partial_t \hat{U} = \hat{H}(t)\,\hat{U}\,. \tag{B.23}$$

Integrating Eq. (B.23), we have to respect time ordering

$$\hat{U}(\Delta t) = 1 + \sum_{n=1}^{\infty} \left(-\frac{i}{\hbar}\right)^n \int_0^{\Delta t} dt_1 \int_0^{t_1} dt_2 \ldots \int_0^{t_{n-1}} dt_n \, \hat{H}(t_1)\, \hat{H}(t_2) \ldots \hat{H}(t_n)\,. \tag{B.24}$$

We can rewriting the Hamiltonian $\hat{H}(t) = \hat{T} + \tilde{V} + \tilde{V}_g$ with the following definitions

$$\tilde{V} = \hat{V} + \hat{V}_g(t) \tag{B.25}$$

$$\tilde{V}_g(t) = \hat{V}_g(t) - \hat{V}_g(0)\,. \tag{B.26}$$

Eq. (B.25) can now be plugged in Eq. (B.24). We are showing the first two integration steps below

$$\int_0^{\Delta t} dt\, \hat{H}(t) = \int_0^{\Delta t} dt \left(\hat{T} + \tilde{V} + \tilde{V}_g(t)\right) \tag{B.27}$$

$$= \left(\hat{T} + \tilde{V}\right) \Delta t + O(\Delta t^2) \tag{B.28}$$

$$\int_0^{\Delta t} dt_1 \int_0^{t_1} dt_2\, \hat{H}(t_1)\, \hat{H}(t_2) = \frac{\Delta t^2}{2} \left(\hat{T} + \tilde{V}\right)^2 + O(\Delta t^3) \tag{B.29}$$

and in the end

$$\hat{U}(\Delta t) = 1 + \sum_{n=1}^{\infty} \left(-\frac{i}{\hbar}\right)^n \left(\hat{T} + \tilde{V}\right)^n \frac{\Delta t^n}{n!} + O(\Delta t^2) \tag{B.30}$$

$$= e^{-\frac{i}{\hbar}\left(\hat{T}+\tilde{V}\right)\Delta t} + O(\Delta t^2)\,. \tag{B.31}$$

To summarize, the Split-Operator Method for the Gross-Pitaevskii equation has an error of $O(\Delta t^2)$ because the term $g\,|\Psi(x, t_n)|^2$ for every time step is being taken to be the term at the beginning of the time step (*i. e.* neglecting the term $\tilde{V}_g(t)$). An implementation in *Mathematica* is shown below.

```
psiListout = {psiI};
Vopf[psin_] := N[Exp[-0.5*I*delt*(modelV + NL*Abs[psin]^2)/hbar]];
Kopf = N[Exp[-0.5*I*delt*hbar*kGridROT*kGridROT]];

For[j = 1, j <= stepsmax, j++,

  psix = Vopf[psie]*psie;
  psik = Chop[InverseFourier[RotateLeft[psix, n/2 - 1]]];
  psix = Chop[Vopf[psie]*RotateRight[Fourier[Kopf*psik], n/2 - 1]];
  psie = psix;
  Clear[psix];
```

```
  If[Mod[j, tout] == 0, psiListout = Append[psiListout, psie]];

  ];
```

In this piece of code `psiI` is the initial wave function. `Vopf[psin_]` denotes the part of the time evolution operator containing the potential energy with the potential `modelV`, the wave function from the time step before `psin` and the strength of the nonlinearity `NL`. `Kopf` is the part of the time evolution operator containing the kinetic energy. The time propagation of the initial wave function is done in the `for`-loop. After every `tout` time steps, the wave function is stored in a list called `psiListout`.